Histone marks regulate the epithelial-to-mesenchymal transition via alternative splicing

Alexandre Segelle, Yaiza Núñez-Álvarez, Andrew Oldfield, Kimberly Webb, Philipp Voigt, Reini Luco

Report

Cell Reports

Histone marks regulate the epithelial-to-mesenchymal transition via alternative splicing

Graphical abstract

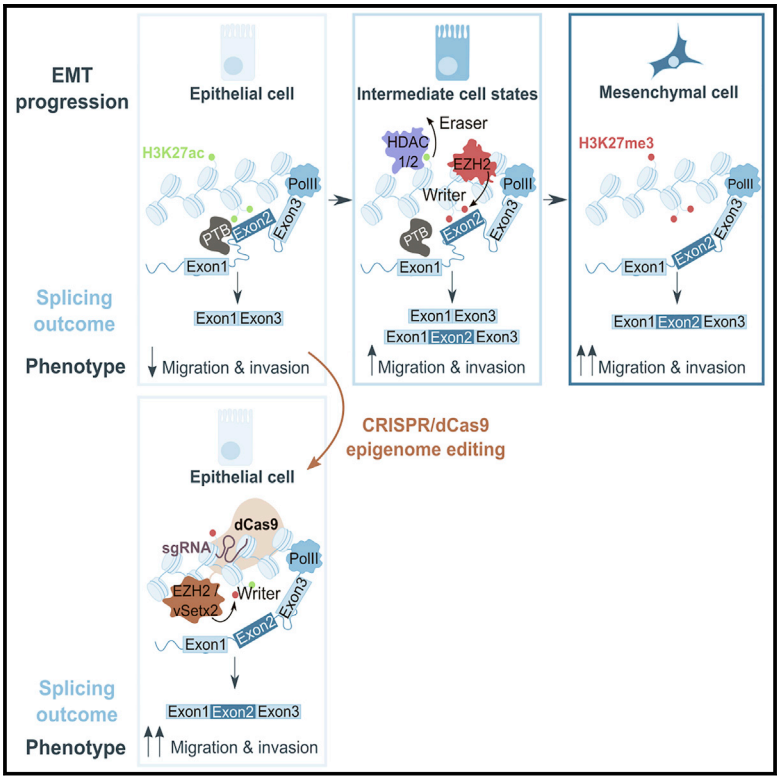

Highlights

- Dynamic changes in specific histone marks correlate with splicing changes during EMT
- Changes in H3K27ac/me3 levels are necessary and sufficient to induce splicing changes
- These exon-specific H3K27 marks regulate PTB recruitment to the pre-mRNA
- Chromatin-induced splicing changes are sufficient to induce an EMT

Authors

Alexandre Segelle, Yaiza Núñez-Álvarez, Andrew J. Oldfield, Kimberly M. Webb, Philipp Voigt, Reini F. Luco

Correspondence

reini.luco@igh.cnrs.fr

In brief

Using epigenome editing tools, Segelle et al. show a driving role for histone marks in establishing the dynamic changes in alternative splicing necessary for EMT reprogramming. The dynamic nature of chromatin modifications helps coordinate rapid changes in alternative splicing that are important for the cell response to a specific stimulus.

Segelle et al., 2022, Cell Reports *38*, 110357
February 15, 2022
https://doi.org/10.1016/j.celrep.2022.110357

CellPress

Cell Reports

CellPress
OPEN ACCESS

Report

Histone marks regulate the epithelial-to-mesenchymal transition via alternative splicing

Alexandre Segelle,[1,3] Yaiza Núñez-Álvarez,[1,3] Andrew J. Oldfield,[1] Kimberly M. Webb,[2] Philipp Voigt,[2] and Reini F. Luco[1,4,*]

[1]Institute of Human Genetics, University of Montpellier, Centre National de la Recherche Scientifique, Montpellier, France
[2]Wellcome Centre for Cell Biology, School of Biological Sciences, University of Edinburgh, Michael Swann Building, Max Born Crescent, Edinburgh EH9 3BF, UK
[3]These authors contributed equally
[4]Lead contact
*Correspondence: reini.luco@igh.cnrs.fr
https://doi.org/10.1016/j.celrep.2022.110357

SUMMARY

Histone modifications impact final splicing decisions. However, there is little evidence of the driving role of these marks in inducing cell-specific splicing changes. Using CRISPR epigenome editing tools, we show in an epithelial-to-mesenchymal cell reprogramming system (epithelial-to-mesenchymal transition [EMT]) that a single change in H3K27ac or H3K27me3 levels right at the alternatively spliced exon is necessary and sufficient to induce a splicing change capable of recapitulating important aspects of EMT, such as cell motility and invasiveness. This histone-mark-dependent splicing effect is highly dynamic and mediated by direct recruitment of the splicing regulator PTB to its RNA binding sites. These results support a role for H3K27 marks in inducing a change in the cell's phenotype via regulation of alternative splicing. We propose the dynamic nature of chromatin as a rapid and reversible mechanism to coordinate the splicing response to cell-extrinsic cues, such as induction of EMT.

INTRODUCTION

During cell reprogramming, such as in epithelial-to-mesenchymal transition (EMT), cell-type-specific transcriptional and splicing programs are tightly regulated to gain new phenotypic traits (Dongre and Weinberg, 2019; Javaid et al., 2013; Pradella et al., 2017; Shapiro et al., 2011; Yang et al., 2016). Alternative splicing depends on the combinatorial recruitment of specific splicing factors to their corresponding RNA binding sites (Daguenet et al., 2015; Hartmann and Valcárcel, 2009). It has long been known that nucleosome positioning and chromatin modifications not only regulate transcriptional programs but also modulate alternative splicing outcomes by impacting RNA polymerase II elongation rates, which in turn impact the kinetics of splicing factor recruitment to competing alternative splice sites in nascent transcripts (Braunschweig et al., 2013; Iannone et al., 2015; de la Mata et al., 2003). More recently, results from our laboratory and others found a more direct role for histone modifications in splicing regulation by modulating the recruitment of specific splicing factors to weaker RNA-binding sites via protein-protein interactions with chromatin-adaptor proteins (Guo et al., 2014; Luco et al., 2010; Pradeepa et al., 2012; Sims et al., 2007; Yearim et al., 2015). At a more global level, recent epigenomic analyses have uncovered a coordinating role for histone modifications in regulating the alternative splicing of specific subsets of genes with common regulatory functions (Agirre et al., 2021). For instance, in acute myeloid leukemia cell lines, a subset of alternatively spliced exons intimately involved in cell proliferation and transformation were regulated by H3K79me2 (Li et al., 2018), whereas during stem cell differentiation, exons involved in cell-cycle progression and DNA-damage responses were specifically marked by H3K36me3 and H3K27ac (Xu et al., 2018). However, most of this evidence is just correlative, or based on genome-wide alterations of the histone mark, which limits the capacity to properly assess the driving role of a localized histone modification in directly inducing a cell-type-specific splicing reprogramming that can phenotypically impact the cell. Neither do we know yet how dynamic changes in splicing are rapidly regulated to establish different cell-type-specific splicing programs in response to a specific signal, such as induction of EMT. There is evidence of dynamic changes in splicing factor expression levels during EMT, such as ESRP1 (Yang et al., 2016). However, many other key splicing regulators are stably expressed during the whole-cell reprogramming, such as PTB and RBFOX2 (Shapiro et al., 2011), and not all ESRP1-dependent splicing events change splicing patterns at the same time points during EMT (Yang et al., 2016), suggesting an additional regulatory layer.

Based on our previous results on the alternatively spliced model gene fibroblast growth factor receptor 2 (*FGFR2*) (Gonzalez et al., 2015; Luco et al., 2010), we are now addressing the dynamic role of chromatin marks in driving the splicing changes necessary to impact the cell's phenotype during EMT cell reprogramming.

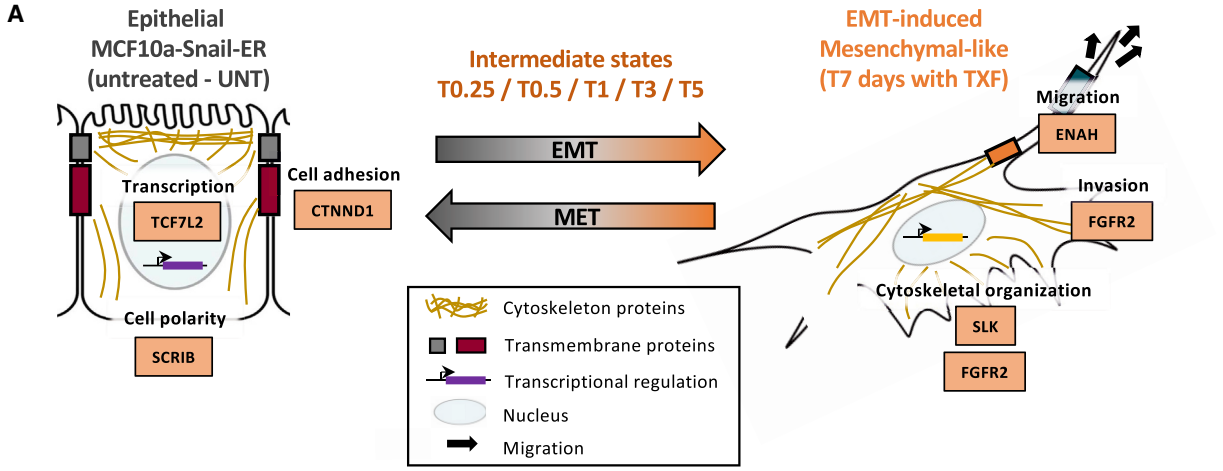

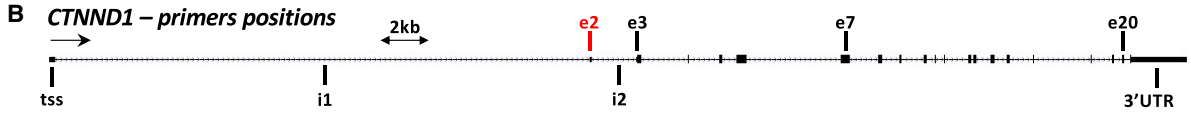

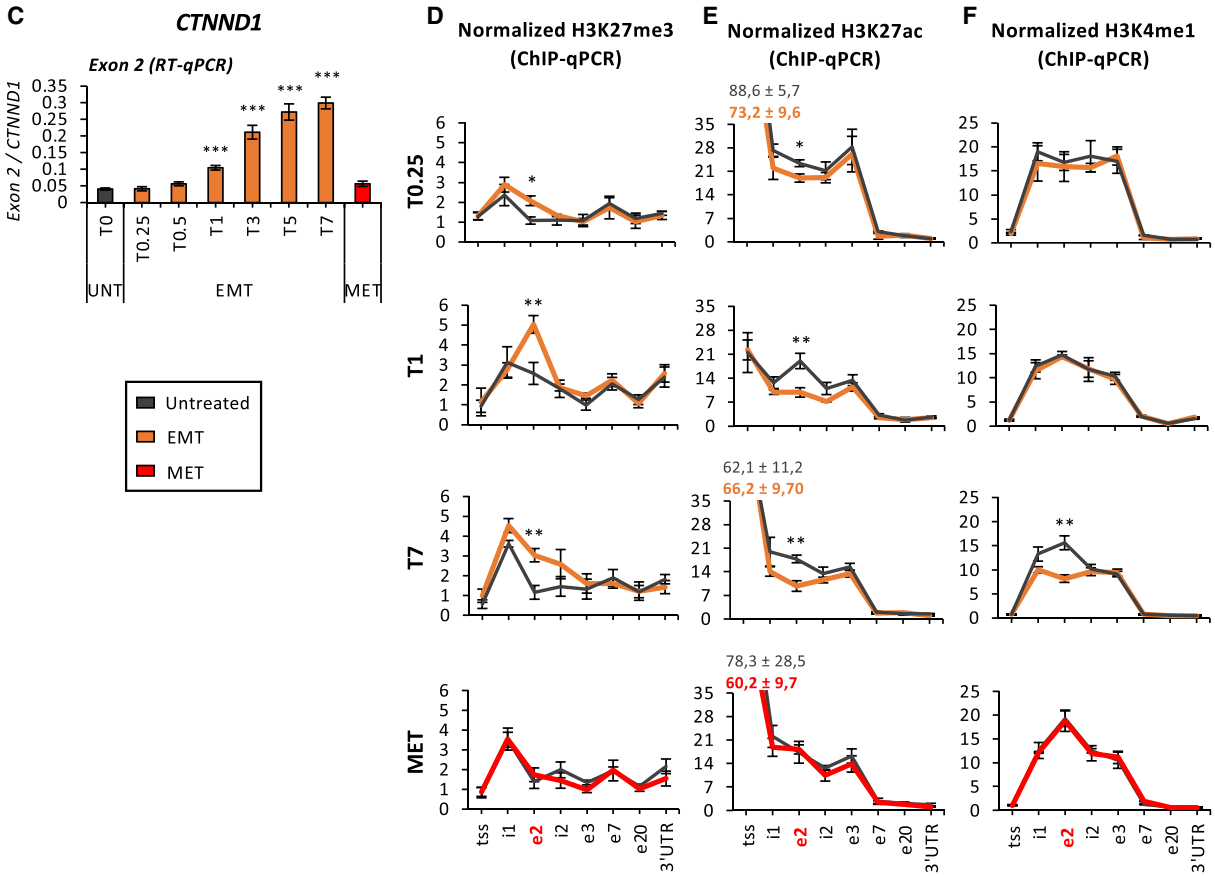

(legend on next page)

RESULTS

Correlation in time between dynamic changes in chromatin modifications and alternative splicing during EMT

EMT is a biological process involved in early development, wound healing, and tumor metastasis (Javaid et al., 2013; Shapiro et al., 2011). Human epithelial MCF10a cells stably expressing the EMT inducer SNAIL1 fused to the estrogen receptor (MCF10a-Snail-ER) can be reprogrammed into mesenchymal-like cells in less than a week by the addition of the ER ligand tamoxifen (Figure 1A) (Javaid et al., 2013). The first changes in splicing of classical EMT genes, such as *FGFR2*, *CTNND1*, *TCF7L2*, *SLK*, *SCRIB*, or *ENAH,* were observed as early as 24 h after induction (T1) (Figures 1C, 2B, S1K, S1N, S1Q, and S1T). Moreover, these changes in splicing could be reversed through a mesenchymal-to-epithelial transition (MET), highlighting the dynamic nature of this cellular system. During induction of EMT, we found a strong correlation in time between dynamic changes in splicing and highly localized changes in H3K27me3, H3K27ac, and H3K4me1 levels in 5 out of 6 studied genes (Figures 1B–1F, 2A–E, and S1K–S1V, summarized in S2A), whereas alternatively spliced exons not changing splicing during EMT, such as *CTNND1* exon 20, did not show changes in these histone marks (Figures 1D–1F and S1B), pointing to an EMT-related splicing effect. Even more, H3K27ac and H3K27me3 changes preceded the changes in splicing (Figures 1D, 1E, 2C, 2D, S1M, and S1P), whereas H3K4me1 correlated with well-established splicing changes at later phases (Figures 1F, 2E, S1M, and S1P). Despite its strong association with alternative splicing (Guo et al., 2014; Luco et al., 2010; Pradeepa et al., 2012), H3K36me3 rarely showed a correlation at the studied exons (Figures S1D, S1I, and S2A; data not shown). These chromatin changes occurred at specific exons within the studied genes and did not correlate in time with major changes in gene expression nor nucleosome positioning (Figures S1A, S1C, S1F, S1H, and S2B), suggesting a splicing-specific effect independent of transcriptional regulation. H3K27me3 and H3K27ac levels were anti-correlated in 3 out of 5 genes analyzed, while H3K4me1 changed in the same direction as H3K27ac, suggesting distinct combinatorial effects in alternative splicing (Figures 1D–1F, 2C–2E, S1K–S1S, and S2A). Furthermore, with the exception of *FGFR2* mutually exclusive exons, H3K27me3 levels were positively correlated with the inclusion of all alternatively spliced exons tested, which points to a coordinating role in the regulation of a specific network with functionally related splicing events (Figure S2A). In support of a role for H3K27 marks in alternative splicing regulation during EMT, we confirmed the enrichment of the polycomb repressive complex 2 (PRC2) member SUZ12, which is involved in H3K27 trimethylation, at the same time points and alternatively spliced exons as the enrichment of H3K27me3 (Figures S1E, S1J, S1L, S1O, S1R, and S1U). This differential binding was not due to changes in overall expression levels of H3K27 chromatin writers (*EZH2* nor *P300*; Figure S2C) but to an exon-specific regulated recruitment of the chromatin effectors to specific genes important for EMT reprogramming. Finally, the observed changes in chromatin modifications were not only as dynamic as the changes in splicing, but were also reversible upon MET, implying plasticity (Figures 1 and 2, MET panels).

In conclusion, we have found a localized enrichment of specific histone marks, H3K27me3 and H3K27ac, whose changes in time precede the highly dynamic splicing changes observed during EMT reprogramming.

Localized changes in H3K27me3 and H3K27ac are sufficient to induce exon-specific changes in alternative splicing

To prove the causal effect of H3K27 marks in splicing, we adapted the CRISPR-dCas9 epigenome editing system (Hilton et al., 2015) to locally change one histone modification at a time, specifically at the differentially marked exon. Catalytic domains of well-known H3K27 modifiers were fused to a DNA targeting-competent, but nuclease-dead, mutant dCas9 to induce site-specific changes in H3K27 methyl or acetyl levels. Using this system, EZH2 H3K27 methyltransferase (Margueron and Reinberg, 2011), UTX1 demethylase (Hong et al., 2007), p300 acetyltransferase (Hilton et al., 2015), and Sid4x deacetylase (Siam et al., 2019) were targeted to *CTNND1* exon 2 or *FGFR2* exon IIIc in untreated epithelial MCF10a-Snail-ER cells (Figures 3A and 3F). To verify the exon specificity of the system, alternatively spliced exons present in the same gene, but not differentially enriched for these histone marks, namely *CTNND1* exon 20 and *FGFR2* exon IIIb, were also targeted using the same dCas9 modifiers (Figures S3A and S3J). H3K27me3 and H3K27ac levels were edited as expected specifically at the targeted exons and regardless of the combination of guide RNAs (gRNAs) used (g1 or g2 against *CTNND1*.ex2 and *FGFR2*.IIIc) (Figures 3B, 3C, 3G, 3H, S3B, S3C, S3F, S3G, S3K, S3L, S3O, and S3P). To improve H3K27me3 editing by dCas9-EZH2, we tested vSET, a viral SET domain protein that specifically methylates H3K27 without the need for PRC2 subunits (Figure S3U) (Mujtaba et al., 2008). A dimeric vSET construct fused to dCas9 (dCas9-vSETx2), but not its catalytic mutant dCas9-vSETx2*, strongly increased H3K27me3 levels precisely at the targeted exons (Figures 3C, 3H, S3C, S3G, S3L, and S3P). Finally, H3K4me1, H3K9ac, and H3K9me2 were not affected by H3K27 epigenome editing, confirming the specificity of the system (Figures S3S and S3T). Interestingly, the increase in H3K27ac levels, mediated by dCas9-p300, also resulted in reduced H3K27me3 levels, while dCas9-vSETx2 reduced H3K27ac (Figures 3B, 3C, 3G, 3H,

Figure 1. Correlation in time between dynamic changes in chromatin modifications and alternative splicing at the *CTNND1* locus during EMT

(A) Schematic representation of EMT and reverse MET.

(B) Scheme of *CTNND1* gene locus with the position of the primers used for ChIP-qPCR. Highlighted in red are the alternatively spliced exons regulated during EMT.

(C) Inclusion levels of *CTNND1* exon 2 relative to total gene expression levels at different time points during EMT and in reversed MET (n = 4 biological replicates).

(D–F) Enrichment levels of H3K27me3, H3K27ac, and H3K4me1 along *CTNND1* locus in EMT-induced cells treated with tamoxifen for 6 h (T0.25), 24 h (T1), or 7 days (T7) and in MET (n = 4). *p < 0.05, **p < 0.01, ***p < 0.001 in two-tail paired Student's t test compared to untreated cells.

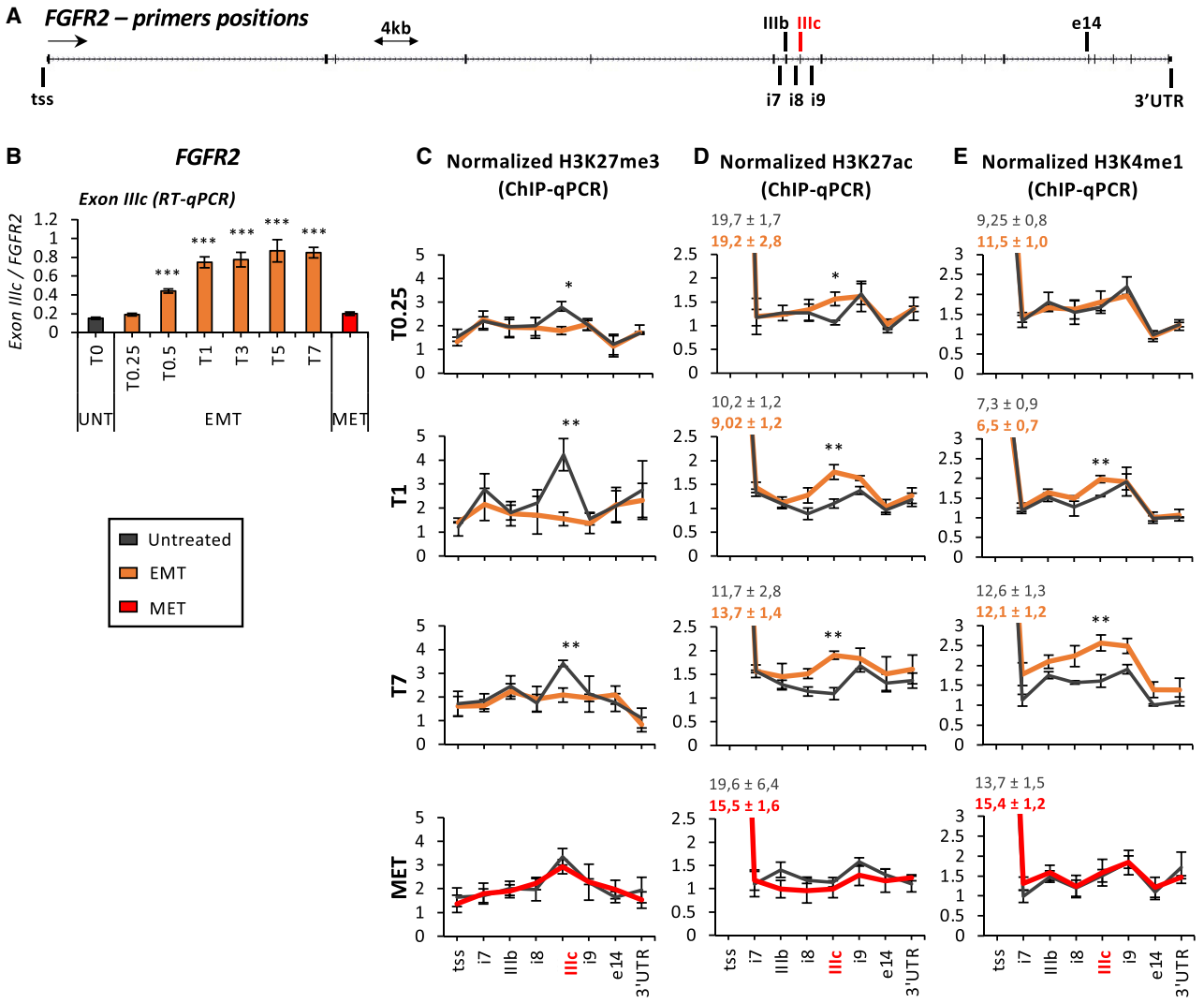

Figure 2. Correlation in time between dynamic changes in chromatin modifications and alternative splicing at the *FGFR2* locus during EMT

(A) Scheme of *FGFR2* gene locus with the position of the primers used for ChIP-qPCR. Highlighted in red are the alternatively spliced exons regulated during EMT. (B) Inclusion levels of *FGFR2* exon IIIc relative to total gene expression levels at different time points during EMT and in reversed MET (n = 4 biological replicates). (C–E) Enrichment levels of H3K27me3, H3K27ac, and H3K4me1 along *FGFR2* locus in EMT-induced cells treated with tamoxifen for 6 h (T0.25), 24 h (T1), or 7 days (T7) and in MET (n = 4). *p < 0.05, **p < 0.01, ***p < 0.001 in two-tail paired Student's t test compared to untreated cells.

S3B, and S3K). These findings confirmed the anti-correlative nature of these histone marks and established the capacity of the CRISPR-dCas9 system to generate the chromatin signatures observed during EMT.

As predicted from the changes in histone modifications observed during EMT (Figures 1D and 1E), only the dCas9-EZH2/vSETx2-mediated increase in H3K27me3 levels, or the dCas9-Sid4x-mediated decrease in H3K27ac, affected *CTNND1* splicing, resulting in a ~3.5-fold increase in the inclusion of the mesenchymal-specific exon 2 (Figure 3D). On the other hand, *FGFR2* exon IIIc splicing was induced by an increase in H3K27ac (dCas9-p300) and a decrease in H3K27me3 (dCas9-UTX1) levels (Figure 3I). H3K27 epigenome editing did not affect total expression levels nor did the splicing of other exons in the same gene, supporting an exon-specific splicing effect (Figures 3E, 3J, S3E, and S3N). Furthermore, the use of catalytically dead mutants, such as dCas9-vSETx2* and dCas9-p300*, did not impact exon inclusion levels either, which validated a histone-mark-dependent splicing effect (Figures 3D and 3I). Finally, targeting *CTNND1* exon 2 or *FGFR2* exon IIIc with a second set of gRNAs (g2) also consistently induced inclusion of the mesenchymal-specific isoform when the corresponding dCas9 modifier was used, confirming the robustness of the results and ruling out potential indirect off-target effects that should be different with each combination of gRNAs (Figures S3A–S3E and S3J–S3N). It is important to note that epigenome editing of alternatively spliced exons not differentially marked by H3K27 modifications during EMT, such as *CTNND1* exon 20, *FGFR2* exon IIIb, or *ENAH*

CellPress
OPEN ACCESS

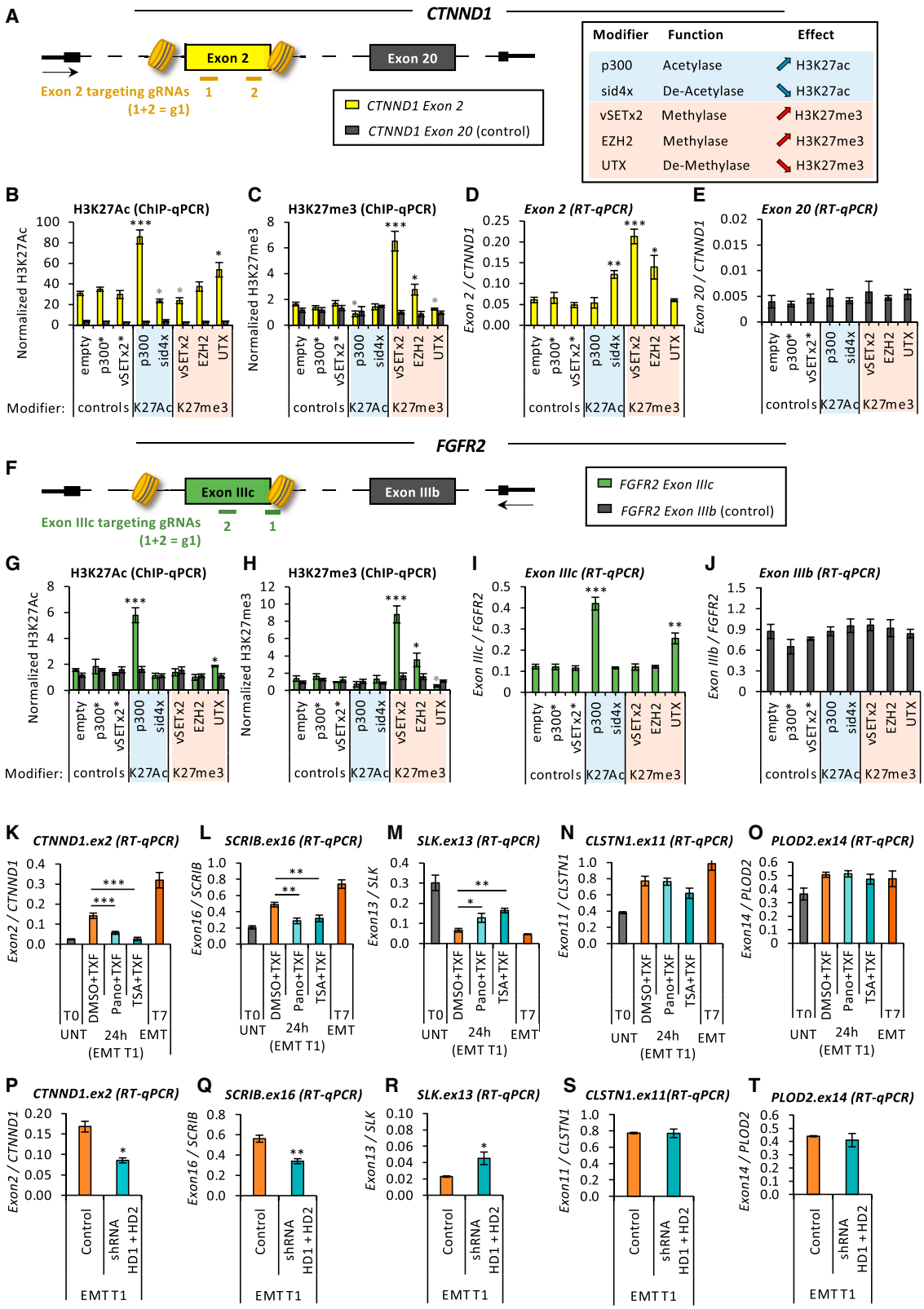

(legend on next page)

exon 11, had no impact on their splicing patterns (Figures S3I and S3R; data not shown), suggesting a context-specific regulatory effect at exons marked by H3K27 modifications.

Taken together, local changes in specific histone modifications at chromatin-marked exons are sufficient to trigger the dynamic changes in alternative splicing observed during EMT. We next sought to study the importance of these dynamic chromatin changes in splicing reprogramming during EMT induction.

Dynamic changes in H3K27ac and H3K27me3 are necessary to induce the splicing changes observed during EMT

To test whether the changes in H3K27 marks are necessary to drive EMT splicing changes, MCF10a-Snail-ER cells were treated with two histone pan-deacetylase inhibitors (HDACi) during EMT induction. Both Trichostatin A and Panobinostat maintained H3K27ac levels significantly higher than in control cells (DMSO) at the studied exons during EMT induction (Figure S4A). Despite a successful EMT (Figure S4B), exons in which there is a depletion in H3K27ac levels and/or an increase in H3K27me3 during EMT, which are *CTNND1* exon 2, *SCRIB* exon 16, and, to a lesser extent, *SLK* exon 13, did not shift to the expected mesenchymal-specific splicing isoform (Figures 3K–3M). In contrast, alternatively spliced exons changing splicing at early time points during EMT, but with no changes in H3K27 marks (in *CLSTN1* and *PLOD2* genes), were not impacted, supporting a specific effect on exons sensitive to H3K27 marks (Figures 3N and 3O). To reduce pleiotropic indirect effects from the inhibitors (Figure S4C) and narrow down the HDACs necessary for dynamic changes in splicing, we specifically knocked down catalytically active HDACs expressed in MCF10a-Snail-ER cells. Only the double knock down of HDAC1 and HDAC2 during EMT induction recapitulated HDACi results without impacting the expression of any of the splicing regulators of relevance for EMT, confirming the driving role of H3K27 marks in inducing specific changes in alternative splicing (Figures 3P–3T and S4D–S4F).

H3K27 marks do not regulate splicing by modulating RNA polymerase II elongation rates

Chromatin has long been proposed to impact splicing by modulating the RNA polymerase II elongation rate (Braunschweig et al., 2013; Luco et al., 2011). As H3K27me3 is known to mediate chromatin compaction, which can slow down transcription kinetics, whereas H3K27ac displays opposite effects on chromatin and RNA polymerase II dynamics (Margueron and Reinberg, 2011; de la Mata et al., 2003), we compared RNA polymerase II elongation rates at *CTNND1* exon 2 before and after EMT induction. As expected, using the RNA polymerase II inhibitor DRB for synchronous pause/release of transcription in a cell population, we found a delay in transcription of *CTNND1* exon 2, but not in the constitutively spliced exon 15, in tamoxifen-induced EMT cells (Figures 4B and 4E). This delay correlated with the enrichment of H3K27me3 and RNA polymerase II at exon 2, which is consistent with a slowdown of RNA polymerase II kinetics (Figures 1D, 4C, and 4F). However, this RNA polymerase II effect was not observed 12 h after induction of EMT (T0.5; Figures 4A and 4D), even though changes in H3K27 marks and exon 2 inclusion were already detected at this time point (Figure 1, T0.25 panels), suggesting that early changes in splicing, dependent on H3K27 marks, are unlikely to be mediated by changes in RNA polymerase II kinetics. Finally, treatment with drugs increasing (Trichostatin A [TSA]) or decreasing (5,6-Dichloro-1-β-D-ribofuranosylbenzimidazole [DRB]) the RNA polymerase II elongation rate did not affect *CTNND1* splicing in steady-state epithelial nor EMT-induced mesenchymal-like cells (Figures S5A and S5B), ruling out an RNA-polymerase-II-mediated effect. We thus conclude that changes in the RNA polymerase II elongation rate do not play a role in establishing the *CTNND1* mesenchymal isoform during EMT, but may be a consequence of the change in the cell-type-specific splicing pattern that could play a role in its maintenance as a feedback mechanism to reinforce the change in splice site choice.

H3K27 marks modulate the direct recruitment of specific splicing factors to the pre-mRNA

In parallel with the RNA polymerase II kinetic model, we and others have identified a more direct role for histone and DNA marks in regulating the recruitment of splicing regulators to the pre-mRNA (Guo et al., 2014; Luco et al., 2010; Pradeepa et al., 2012; Sims et al., 2007; Yearim et al., 2015). To identify the splicing factors involved in the H3K27-mediated regulation of splicing, we first tested a panel of regulators potentially involved in *CTNND1* exon 2 splicing. Short hairpin RNA (shRNA)-mediated knock down of all the RNA binding proteins previously implicated in *CTNND1* splicing regulation (Girardot et al., 2018; Tripathi et al., 2016; Warzecha et al., 2010), or identified by motif search analysis, pointed to the splicing factor PTB as the major repressor of *CTNND1* exon 2 inclusion (Figures 4G, 4H, and S5C). UV-crosslinked RNA immunoprecipitation assays further revealed the differential recruitment of PTB to exon 2 pre-mRNA during EMT, with preferential binding to the H3K27ac-marked exon in untreated epithelial MCF10a-Snail-ER cells,

Figure 3. H3K27 marks are necessary and sufficient to induce a change in splicing

(A and F) Schematic representation of *CTNND1* exon 2 and control exon 20 or *FGFR2* exon IIIc and control IIIb with nucleosome and gRNA positions.

(B, C, G, and H) H3K27ac and H3K27me3 enrichment levels at exon 2, exon 20, IIIc, or IIIb in MCF10a-Snail-ER cells infected with different dCas9 epigenomic modifiers and exon-specific gRNAs targeting exon 2 or IIIc (see summary table on the right, n = 4 biological replicates). Empty dCas9, mutated p300*, and vSETx2* were used as negative controls.

(D, E, I, and J) Inclusion levels of *CTNND1* exon 2, exon 20 and *FGFR2* exon IIIb, IIIc in MCF10a-Snail-ER cells infected with dCas9 modifiers and exon 2- or exon IIIc-specific gRNAs (n = 4).

(K–O) Inclusion levels of H3K27-marked exons (in *CTNND1*, *SCRIB*, and *SLK*) and control exons (in *CLSTN1* and *PLOD2*) in EMT-induced cells treated for 24 h with Panobinostat (Pano) or Trichostatin A (TSA) HDAC inhibitors (n = 3).

(P–T) Inclusion levels of the same exons as in (K)–(O) in EMT-induced double knockdown cells for *HDAC1* (HD1) and *HDAC2* (HD2) (n = 3). Non-targeting shRNA was used as a control. *p < 0.05, **p < 0.01, ***p < 0.001 in two-tail paired Student's t test compared to empty dCas9, T1 DMSO, or T1 control shRNA. Black asterisks show a significant increase, while gray asterisks show a significant decrease, in H3K27me3 or H3K27ac levels.

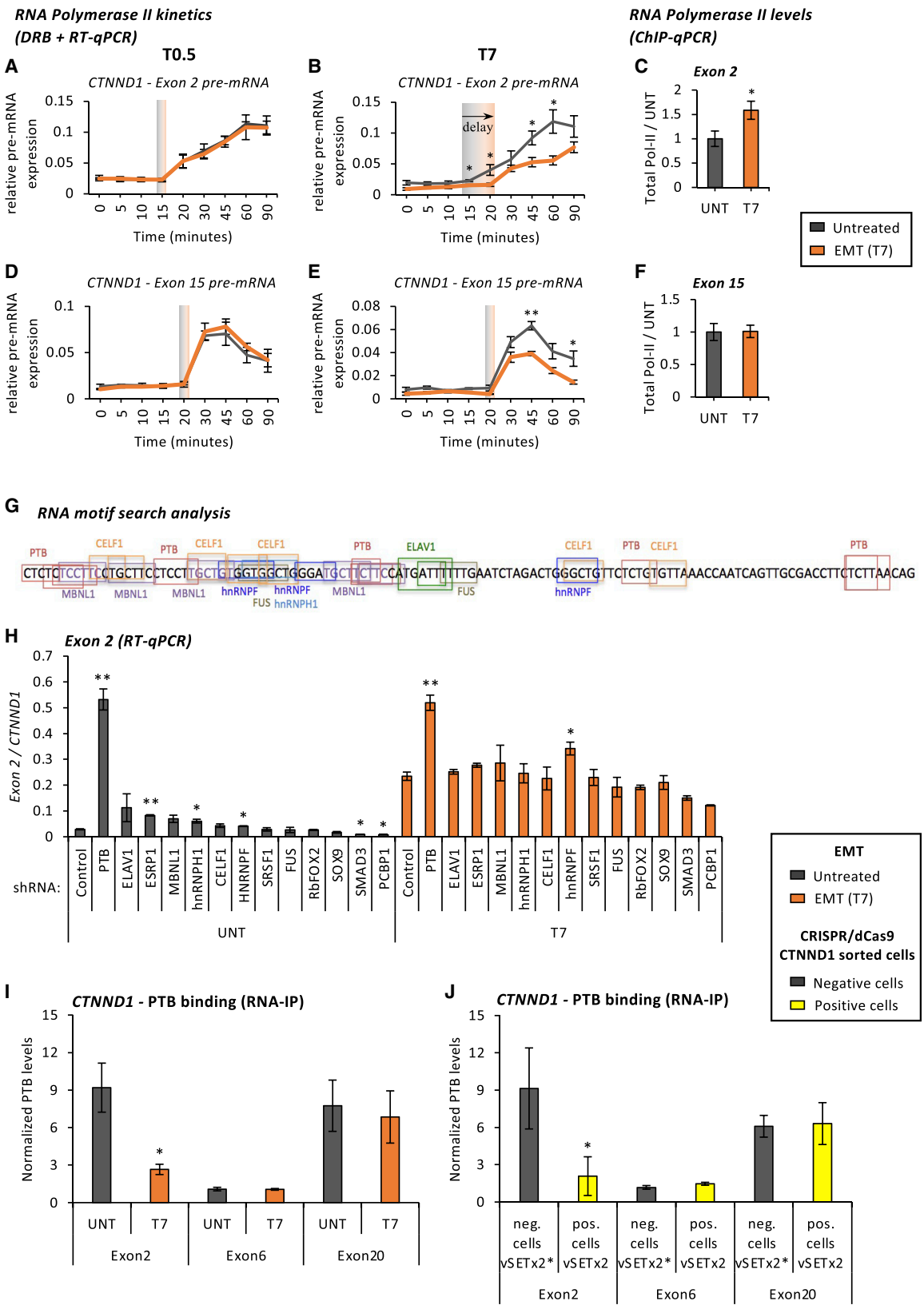

(legend on next page)

when the exon is excluded (Figures 4I and S5D). We next assessed the impact of altering H3K27ac/me3 levels, using the dCas9-vSETx2 construct, on PTB recruitment to *CTNND1* exon 2 in epithelial MCF10a-Snail-ER cells. As predicted, a local increase in H3K27me3 levels at *CTNND1* exon 2, which increases exon inclusion, reduced PTB binding to the exon pre-mRNA, whereas PTB binding to control regions, such as *CTNND1* exon 6 and exon 20, was not affected (Figures 4J and S5E). Of note, all exons found to be sensitive to H3K27 marks, namely *FGFR2* exon IIIb/IIIc, *SCRIB* exon 16, *SLK* exon 13, and *TCF7L2* exon 4, were also dependent on PTB levels (Figures S5F–S5H; Luco et al., 2010). Even more, PTB knockdown recapitulated the splicing phenotype observed when H3K27ac levels were low and/or when H3K27me3 levels were high, supporting a direct effect of H3K27 marks on PTB recruitment (Figures 1, S1, 4H, and S5F–S5H).

We thus conclude that in the genes studied, dynamic changes in H3K27 marks directly impact alternative splicing by modulating PTB recruitment to the pre-mRNA.

Chromatin-induced changes in splicing recapitulate the EMT

The physiological impact of chromatin-mediated changes in splicing have long been controversial. Changes in *CTNND1* and *FGFR2* alternative splicing are important regulators of EMT, and their mesenchymal-specific isoforms have been associated with poor prognosis in several carcinomas, including breast and prostate cancers (Carstens et al., 1997; Sebestyén et al., 2015; Shapiro et al., 2011; Villemin et al., 2021). An increase in *CTNND1* exon 2 inclusion levels affects the capacity of the protein to interact with E-cadherins, destabilizing cell-cell interactions and increasing cell motility and invasiveness (Yanagisawa et al., 2008). Alternatively, an H3K36me3-mediated decrease of *FGFR2* exon IIIc mesenchymal isoform, which impacts the ligand specificity of the receptor, was shown to significantly decrease the migratory and invasive phenotype of non-small lung cancer cells without impacting proliferation or apoptosis (Sanidas et al., 2014). We thus tested whether H3K27-mediated induction of the mesenchymal-specific isoform of *CTNND1* or *FGFR2* would be sufficient to reproduce migratory EMT-like phenotypes in epithelial MCF10-Snail-ER cells.

A dCas9-Sid4x- or dCas9-vSETx2-mediated increase in *CTNND1*.ex2 mesenchymal isoform and a dCas9-p300- or dCas9-UTX1-mediated increase in *FGFR2*.IIIc significantly decreased the expression of classical epithelial markers, such as *E-cadherin* and epithelial cellular adhesion molecule (EPCAM), while increasing the expression of the mesenchymal markers *ECM-1* and melanoma cell adhesion molecule (MCAM) by ~2-fold both at the transcript and protein levels (Figures 5A–5D). This was specific to the targeting of the appropriate dCas9 epigenomic modifier to the corresponding alternatively spliced exon, since none of the other dCas9 modifiers nor the dCas9 mutants had an effect on EMT when targeted to *FGFR2* or *CTNND1* H3K27-marked exons (Figures S6A–S6F). Neither did the targeting of other alternatively spliced exons, such as *FGFR2*.IIIb, *CTNND1*.ex20, or *ENAH*.ex11, with a dCas9 modifier impacting *FGFR2* or *CTNND1* splicing have an effect on EMT (Figures S6A–S6F). In support of these observations, the H3K27me3-mediated shift in *CTNND1* splicing significantly increased the non-directional (wound healing) and directional (Transwell assay) migration capacity of targeted MCF10a-Snail-ER cells, whereas catalytically dead dCas9-vSETx2* had no effect (Figures 5E–5G). None of the splicing, nor the transcriptional, regulators known to play a role in EMT changed expression levels upon CRISPR epigenome editing (Figures S6G and S6H), supporting a direct chromatin-mediated effect on the EMT phenotype. However, CRISPR-dCas9 editing systems are known to be heterogeneous, with just a percentage of cells properly targeted at the gene locus of interest. To assess the real biological impact of chromatin-induced changes in CTNND1 splicing, we sorted cells in which the mesenchymal-specific protein variant was present using a splicing-specific antibody recognizing only the CTNND1 protein isoform including exon 2 (mCTNND1(ex2)). dCas9-vSETx2-mediated induction of exon 2 inclusion in epithelial MCF10a-Snail-ER cells increased the proportion of cells expressing the CTNND1 mesenchymal protein isoform almost as much as the tamoxifen-induced EMT cells (31% versus 43% positive cells, respectively), whereas the use of the dCas9-vSETx2* mutant had no effect (9% of positive cells as in epithelial cells) (Figure 5H). Moreover, mCTNND1(ex2)-positive cells from dCas9-vSETx2-infected cells, but not dCas9-vSETx2*-infected cells, included exon 2 at similar levels as in EMT cells (Figure S6J), supporting a complete splicing switch to the mesenchymal phenotype only when inducing changes in H3K27 marks. In concordance, EMT was now completely recapitulated, with changes in directional migration, invasion, and expression of EMT markers similar to the ones observed in tamoxifen-induced cells (Figures 5I–5M). To further rule out indirect off-target effects, an independent combination of gRNAs targeting exon 2 (g2), which should have different off targets,

Figure 4. H3K27 marks regulate PTB recruitment to the pre-mRNA

(A, B, D, and E) Apparition in time of *CTNND1* exon 2 or control exon 15 pre-mRNA in synchronized untreated and tamoxifen-induced cells upon release of the transcriptional inhibitor DRB after 0.5 days (T0.5) or 7 days (T7) of EMT induction. qRT-PCR results are normalized by tRNA expression levels (n = 3 biological replicates).

(C and F) Total RNA polymerase II levels at *CTNND1* exon 2 and control exon 15 in untreated and tamoxifen-induced cells (n = 3). The percentage of input is represented relative to untreated cells.

(G) Predicted RNA-binding motifs along *CTNND1* exon 2 pre-mRNA in at least two of the four softwares used.

(H) *CTNND1* exon 2 inclusion levels upon shRNA knock down of candidate splicing regulators in untreated and tamoxifen-induced T7 cells (n = 3).

(I) PTB enrichment levels at *CTNND1* exon 2 pre-mRNA in untreated and tamoxifen-induced T7 cells. Constitutively included *CTNND1* exon 6 and excluded exon 20 were used as controls. The percentage of input was normalized by immunoglobulin G (IgG) and control *CTNND1* exon 7 levels (n = 5).

(J) PTB enrichment levels in cell-sorted cells expressing (positive) or not (negative) the mesenchymal-specific splicing isoform mCTNND1(ex2) in MCF10a-Snail-ER cells infected with dCas9-vSETx2 or mutant dCas9-vSETx2* and exon2-specific gRNAs (g1, n = 6). *p < 0.05, **p < 0.01, ***p < 0.001 in two-tail paired Student's t test compared to control cells (untreated, non-targeting shRNA or negative).

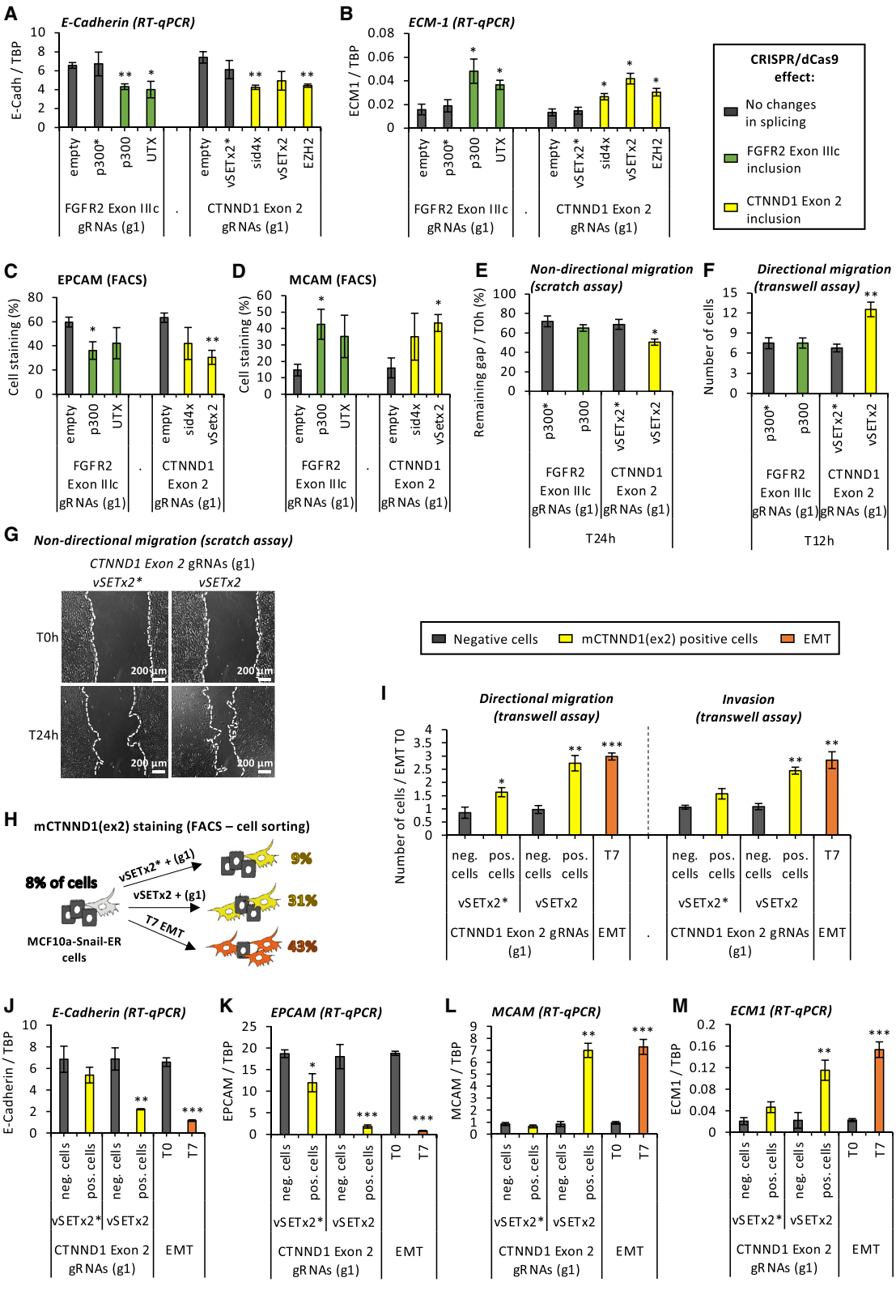

(legend on next page)

had comparable biological effects (Figures S6I–S6N), reinforcing a direct role for chromatin-induced splicing changes in driving important aspects of EMT cell reprogramming.

DISCUSSION

Our results support a model by which local changes in exon-specific H3K27 modifications are responsible for the dynamic changes in alternative splicing necessary for cell reprogramming. It also raises the intriguing question of whether chromatin modifications might be responsible for the rapid and coordinated splicing reprogramming necessary for the acquisition of new phenotypic traits in response to cell-extrinsic cues, like EMT induction. In fact, plants and flies already exploit these chromatin- and splicing-mediated mechanisms to respond to changes in light and temperature (Martin Anduaga et al., 2019; Pajoro et al., 2017; Petrillo et al., 2014). Mammalian cells likely take advantage of the same systems by epigenomically regulating key splicing events for a more efficient and rapid response to external stimuli. Surprisingly, not all histone marks showed the same dynamics during EMT. For instance, H3K4me1 only correlated with late changes in splicing, similar to RNA polymerase II elongation rates. Since H3K4me1 levels have been positively associated with RNA polymerase II kinetics (Jonkers et al., 2014), we propose that, contrary to H3K27 marks, H3K4me1 changes could be a consequence of altered splicing, setting up a regulatory feedback loop to reinforce or maintain cell-type-specific splicing patterns.

Chromatin is known to impact splicing by modulating the recruitment of the splicing machinery to weaker RNA binding sites. Here, we show a direct role for H3K27 acetylation in inducing recruitment of PTB to its target exons, independently of RNA polymerase II kinetics. PTB has already been shown to interact with histone marks via chromatin-binding proteins, such as MRG15, at specific gene loci such as *FGFR2* (Luco et al., 2010). We have shown in the past that PTB recruitment to *FGFR2* exon IIIb is regulated by H3K27me3 and H3K36me2,3 levels, which determine whether the chromatin-adaptor complex MRG15-PTB can be recruited to the chromatin/RNA, thus impacting *FGFR2* splicing (Gonzalez et al., 2015; Luco et al., 2010). In the case of *CTNND1*, MRG15 does not play a role in exon 2 splicing, suggesting that other H3K27ac-binding chromatin/adaptor complexes might exist. Alternatively, splicing factors, such as hnRNPA2B1 or hnRNPL, have also been reported to directly interact with native chromatin in an RNA-independent way (Luco et al., 2011; Pradeepa et al., 2012; Thompson et al., 2015; Kfir et al., 2015; Yearim et al., 2015) or via physical interaction with chromatin modifiers, such as RBFOX2 and PRC2 (Wei et al., 2016). Intriguingly, histone mark writers, such as p300, have recently been shown to modulate alternative splicing by post-translationally acetylating the splicing factors themselves, which can impact their RNA binding capacity and activity (Siam et al., 2019). There is evidence of a p300-mediated acetylation of PTB (Weinert et al., 2018), although its functional impact, as well as the existence of other post-translational modifications such as methylation, remain unclear.

Finally, we expect this chromatin-mediated regulation of alternative splicing to be gene- and context specific. In a recently published genome-wide analysis, using the most extensive epigenomic and transcriptomic datasets publicly available from the ENCODE and Epigenomic Roadmap projects, we showed that exons differentially marked by specific chromatin modifications share common functional and regulatory pathways, suggesting a coordinating role for histone marks in regulating the alternative splicing of functionally related genes (Agirre et al., 2021). In the case of H3K27ac and H3K27me3, we have identified several alternatively spliced genes (*FGFR2*, *CTNND1*, *TCF7L2*, *SLK*, *SCRIB*) intimately involved in cell migration and invasion whose alternative splicing depends on H3K27 marks and PTB (Pradella et al., 2017; Roovers et al., 2009; Sanidas et al., 2014; Wenzel et al., 2020; Yanagisawa et al., 2008). We thus propose that H3K27 marks coordinate the reprogramming of functionally related splicing events necessary to induce, in a dynamic and reversible way, phenotypic traits characteristic of EMT. In addition to the H3K27-centric regulation of EMT-related alternative splicing identified here, other histone marks might also coordinate the regulation of alternative splicing events important for other physiological processes. Future studies will bring necessary insights into this highly dynamic regulatory layer.

Limitations of the study

CRISPR-dCas9-mediated epigenome editing is highly specific and reproducible, with a low impact of potential off targets. However, it can also be inefficient and heterogeneous. First, several targeting gRNAs and chromatin writers' catalytic domains have to be tried until the best editing combination is identified. Second, the percentage of cells in which dCas9 is efficiently editing the epigenome can vary between dCas9 modifiers. dCas9-vSET almost recapitulated *CTNND1* mesenchymal-specific splicing levels in epithelial cells. However, dCas9-EZH2 failed to do so, and in the case of *FGFR2*, dCas9-p300 just induced a splicing change comparable to the one observed at very early time points during EMT reprogramming, which was insufficient to impact the cell's phenotype.

Figure 5. Chromatin-induced splicing changes recapitulate an EMT

(A–D) Expression levels of epithelial (*E-cadherin*, EPCAM) and mesenchymal (*ECM1*, MCAM) markers at the mRNA and protein levels in MCF10a-Snail-ER cells infected with key dCas9 modifiers and *FGFR2* exon-IIIc- or *CTNND1* exon-2-specific gRNAs (n = 4 biological replicates).

(E–G) Functional EMT assays to test non-directional (scratch assay) and directional (Transwell) migration in MCF10-Snail-ER cells infected with dCas9 modifiers and IIIc- or exon 2-specific targeting gRNAs (n = 3).

(H–I) Cell sorting of MCF10a-Snail-ER cells infected with exon 2-targeting gRNAs and either dCas9-vSETx2 or mutant dCas9-vSETx2* using a CTNND1 splicing-specific antibody for directional migration and invasion assays. The percentage of mCTNND1(ex2)-positive cells is shown on the right (H). Negative cells were used as control (Neg). The number of migrating or invading sorted cells were normalized to untreated cells (T0) for comparison with T7-induced EMT cells (n = 3).

(J–M) Expression levels of epithelial (*E-cadherin*, *EPCAM*) and mesenchymal (*MCAM*, *ECM1*) markers in cell-sorted MCF10a-Snail-ER cells as in (H) (n = 3).

*p < 0.05, **p < 0.01, ***p < 0.001 in two-tail paired Student's t test compared to the corresponding control (empty, vSETx2*, or negative cells).

It is also possible that additional chromatin mechanisms, such as the aforementioned dependence on H3K36me3 marks, could limit the capacity to edit *FGFR2* splicing by just editing one single histone mark. It would be interesting to test the impact on splicing and EMT of combining more than one chromatin modifier at a specific exon to recapitulate this chromatin complexity. Finally, another important limitation of the study is the cell heterogeneity characteristic of the model system used. EMT is known to be a progressive reprogramming system with several intermediate states that are reflected in the absence of absolute changes in the alternative splicing of most of the genes analyzed. When looking at the global impact of H3K27 marks in PTB-dependent genes, and the mechanisms involved, we faced this cell-to-cell splicing heterogeneity, which underestimated the impact of H3K27 marks in alternative splicing during EMT reprogramming when using average chromatin immunoprecipitation sequencing (ChIP-seq) levels in bulk cells. The use of state-of-the-art single-cell genomics will help elucidate the functional link and the chromatin proteins involved in this H3K27-mediated regulation of alternative splicing relevant for the cell's phenotype.

STAR★METHODS

Detailed methods are provided in the online version of this paper and include the following:

- KEY RESOURCES TABLE
- RESOURCE AVAILABILITY
  - Lead contact
  - Materials availability
  - Data and code availability
- EXPERIMENTAL MODEL AND SUBJECT DETAILS
  - Cell lines and cell culture
  - Cloning and plasmids
  - Expression and purification of vSET constructs
- METHOD DETAILS
  - Methyltransferase assays
  - Epigenome editing
  - Recombinant lentivirus production
  - Chromatin immunoprecipitation
  - RNA extraction and RT-qPCR
  - Migration and invasion assays
  - Flow cytometry
  - Cell sorting - FACS
  - Polymerase II elongation measurement
  - TSA, panobinostat and DRB treatments
  - MNase protection assay for nucleosome positioning
  - shRNA knock-down
  - UV cross-linked RNA-immunoprecipitation
  - RNA motif search analysis
- QUANTIFICATION AND STATISTICAL ANALYSIS

SUPPLEMENTAL INFORMATION

Supplemental information can be found online at https://doi.org/10.1016/j.celrep.2022.110357.

ACKNOWLEDGMENTS

We are thankful to Dr. Haber for the EMT cellular model, to Drs. Bertrand, Salton, Duckett, Pradeepa, and Ge for plasmids, and to Paola Scaffidi and Bernard de Massy for critical reading and discussion of the manuscript. This work was supported by the ANR program Labex EpiGenMed, La Ligue contre le Cancer, the French National Institute of Cancer (INCa PLBIO18-156), and the ANR Young Investigator grant (ANR-16-CE12-0012-01) to the R.F.L. lab and by the Wellcome Trust (104175/Z/14/Z), the Sir Henry Dale Fellowship, and by funding from the European Research Council (ERC-STG no. 639253) to the P.V. lab. We are grateful to Montpellier's MRI imaging facility and Edinburgh's Protein Production Facility for their support.

AUTHOR CONTRIBUTIONS

Conceptualization, A.S., Y.N.-A., and R.F.L.; methodology and investigation: A.S., Y.N.-A., and K.M.W.; writing & editing, A.S., Y.N.-A., A.J.O., P.V., and R.F.L.; funding acquisition, P.V. and R.F.L.

DECLARATION OF INTERESTS

The authors declare no competing interests.

Received: May 21, 2021
Revised: September 20, 2021
Accepted: January 19, 2022
Published: February 15, 2022

REFERENCES

Agirre, E., Oldfield, A., Bellora, N., Segelle, A., and Luco, R.F. (2021). Splicing-associated chromatin signatures: a combinatorial and position-dependent role for histone marks in splicing definition. Nat. Commun. *12*, 682.

Braunschweig, U., Gueroussov, S., Plocik, A.M., Graveley, B.R., and Blencowe, B.J. (2013). Dynamic integration of splicing within gene regulatory pathways. Cell *152*, 1252–1269.

Carstens, R.P., Eaton, J.V., Krigman, H.R., Walther, P.J., and Garcia-Blanco, M.A. (1997). Alternative splicing of fibroblast growth factor receptor 2 (FGF-R2) in human prostate cancer. Oncogene *15*, 3059–3065.

Daguenet, E., Dujardin, G., and Valcarcel, J. (2015). The pathogenicity of splicing defects: mechanistic insights into pre-mRNA processing inform novel therapeutic approaches. EMBO Rep. *16*, 1640–1655.

Dongre, A., and Weinberg, R.A. (2019). New insights into the mechanisms of epithelial–mesenchymal transition and implications for cancer. Nat. Rev. Mol. Cell Biol. *20*, 69–84.

Girardot, M., Bayet, E., Maurin, J., Fort, P., Roux, P., and Raynaud, P. (2018). SOX9 has distinct regulatory roles in alternative splicing and transcription. Nucleic Acids Res. *46*, 9106–9118.

Gonzalez, I., Munita, R., Agirre, E., Dittmer, T.A., Gysling, K., Misteli, T., and Luco, R.F. (2015). A lncRNA regulates alternative splicing via establishment of a splicing-specific chromatin signature. Nat. Struct. Mol. Biol. *22*, 370–376.

Guo, R., Zheng, L., Park, J.W., Lv, R., Chen, H., Jiao, F., Xu, W., Mu, S., Wen, H., Qiu, J., et al. (2014). BS69/ZMYND11 reads and connects histone H3.3 lysine 36 trimethylation-decorated chromatin to regulated pre-mRNA processing. Mol. Cell *56*, 298–310.

Ha, K., Fiskus, W., Choi, D.S., Bhaskara, S., Cerchietti, L., Devaraj, S.G.T., Shah, B., Sharma, S., Chang, J.C., Melnick, A.M., et al. (2014). Histone deacetylase inhibitor treatment induces 'BRCAness' and synergistic lethality with PARP inhibitor and cisplatin against human triple negative breast cancer cells. Oncotarget *5*, 5637–5650.

Hartmann, B., and Valcárcel, J. (2009). Decrypting the genome's alternative messages. Curr. Opin. Cell Biol. *21*, 377–386.

Hilton, I.B., D'Ippolito, A.M., Vockley, C.M., Thakore, P.I., Crawford, G.E., Reddy, T.E., and Gersbach, C.A. (2015). Epigenome editing by a CRISPR-

Cas9-based acetyltransferase activates genes from promoters and enhancers. Nat. Biotechnol. *33*, 510–517.

Hong, S., Cho, Y.-W., Yu, L.-R., Yu, H., Veenstra, T.D., and Ge, K. (2007). Identification of JmjC domain-containing UTX and JMJD3 as histone H3 lysine 27 demethylases. PNAS *104*, 18439–18444.

Hwang, C., Giri, V.N., Wilkinson, J.C., Wright, C.W., Wilkinson, A.S., Cooney, A.K., and Duckett, C.S. (2008). EZH2 regulates the transcription of estrogen-responsive genes through association with REA, an estrogen receptor corepressor. Breast Cancer Res Treat *107* (*2*), 235–242.

Iannone, C., Pohl, A., Papasaikas, P., Soronellas, D., Vicent, G.P., Beato, M., and Valcárcel, J. (2015). Relationship between nucleosome positioning and progesterone-induced alternative splicing in breast cancer cells. RNA *21*, 360–374.

Javaid, S., Zhang, J., Anderssen, E., Black, J.C., Wittner, B.S., Tajima, K., Ting, D.T., Smolen, G.A., Zubrowski, M., Desai, R., et al. (2013). Dynamic chromatin modification sustains epithelial-mesenchymal transition following inducible expression of snail-1. Cell Rep. *5*, 1679–1689.

Jonkers, I., Kwak, H., and Lis, J.T. (2014). Genome-wide dynamics of Pol II elongation and its interplay with promoter proximal pausing, chromatin, and exons. Elife *3*, e02407.

Kfir, N., Lev-Maor, G., Glaich, O., Alajem, A., Datta, A., Sze, S.K., Meshorer, E., and Ast, G. (2015). SF3B1 association with chromatin determines splicing outcomes. Cell Rep. *11*, 618–629.

Li, T., Liu, Q., Garza, N., Kornblau, S., and Jin, V.X. (2018). Integrative analysis reveals functional and regulatory roles of H3K79me2 in mediating alternative splicing. Genome Med. *10*, 30.

Luco, R.F., Pan, Q., Tominaga, K., Blencowe, B.J., Pereira-Smith, O.M., and Misteli, T. (2010). Regulation of alternative splicing by histone modifications. Science *327*, 996–1000.

Luco, R.F., Allo, M., Schor, I.E., Kornblihtt, A.R., and Misteli, T. (2011). Epigenetics in alternative pre-mRNA splicing. Cell *144*, 16–26.

Manzur, K.L., Farooq, A., Zeng, L., Plotnikova, O., Koch, A.W., Sachchidanand, and Zhou, M.-M. (2003). A dimeric viral SET domain methyltransferase specific to Lys27 of histone H3. Nat. Struct. Biol. *10*, 187–196.

Margueron, R., and Reinberg, D. (2011). The polycomb complex PRC2 and its mark in life. Nature *469*, 343–349.

Martin Anduaga, A., Evantal, N., Patop, I.L., Bartok, O., Weiss, R., and Kadener, S. (2019). Thermosensitive alternative splicing senses and mediates temperature adaptation in Drosophila. Elife *8*, e44642.

de la Mata, M., Alonso, C.R., Kadener, S., Fededa, J.P., Blaustein, M., Pelisch, F., Cramer, P., Bentley, D., and Kornblihtt, A.R. (2003). A slow RNA polymerase II affects alternative splicing in vivo. Mol. Cell *12*, 525–532.

Mujtaba, S., Manzur, K.L., Gurnon, J.R., Kang, M., Van Etten, J.L., and Zhou, M.-M. (2008). Epigenetic transcriptional repression of cellular genes by a viral SET protein. Nat. Cell Biol. *10*, 1114–1122.

Pajoro, A., Severing, E., Angenent, G.C., and Immink, R.G.H. (2017). Histone H3 lysine 36 methylation affects temperature-induced alternative splicing and flowering in plants. Genome Biol. *18*, 102.

Petrillo, E., Godoy Herz, M.A., Fuchs, A., Reifer, D., Fuller, J., Yanovsky, M.J., Simpson, C., Brown, J.W.S., Barta, A., Kalyna, M., et al. (2014). A chloroplast retrograde signal regulates nuclear alternative splicing. Science *344*, 427–430.

Pradeepa, M.M., Sutherland, H.G., Ule, J., Grimes, G.R., and Bickmore, W.A. (2012). Psip1/Ledgf p52 binds methylated histone H3K36 and splicing factors and contributes to the regulation of alternative splicing. PLoS Genet. *8*, e1002717.

Pradella, D., Naro, C., Sette, C., and Ghigna, C. (2017). EMT and stemness: flexible processes tuned by alternative splicing in development and cancer progression. Mol. Cancer *16*, 8.

Roovers, K., Wagner, S., Storbeck, C.J., O'Reilly, P., Lo, V., Northey, J.J., Chmielecki, J., Muller, W.J., Siegel, P.M., and Sabourin, L.A. (2009). The Ste20-like kinase SLK is required for ErbB2-driven breast cancer cell motility. Oncogene *28*, 2839–2848.

Sanidas, I., Polytarchou, C., Hatziapostolou, M., Ezell, S.A., Kottakis, F., Hu, L., Guo, A., Xie, J., Comb, M.J., Iliopoulos, D., et al. (2014). Phosphoproteomics screen reveals akt isoform-specific signals linking RNA processing to lung cancer. Mol. Cell *53*, 577–590.

Sebestyén, E., Zawisza, M., and Eyras, E. (2015). Detection of recurrent alternative splicing switches in tumor samples reveals novel signatures of cancer. Nucleic Acids Res. *43*, 1345–1356.

Shapiro, I.M., Cheng, A.W., Flytzanis, N.C., Balsamo, M., Condeelis, J.S., Oktay, M.H., Burge, C.B., and Gertler, F.B. (2011). An EMT-driven alternative splicing program occurs in human breast cancer and modulates cellular phenotype. PLoS Genet. *7*, e1002218.

Siam, A., Baker, M., Amit, L., Regev, G., Rabner, A., Najar, R.A., Bentata, M., Dahan, S., Cohen, K., Araten, S., et al. (2019). Regulation of alternative splicing by p300-mediated acetylation of splicing factors. RNA *25*, 813–824.

Sims, R.J., Millhouse, S., Chen, C.F., Lewis, B.A., Erdjument-Bromage, H., Tempst, P., Manley, J.L., and Reinberg, D. (2007). Recognition of trimethylated histone H3 lysine 4 facilitates the recruitment of transcription postinitiation factors and pre-mRNA splicing. Mol. Cell *28*, 665–676.

Thompson, P.J., Dulberg, V., Moon, K.M., Foster, L.J., Chen, C., Karimi, M.M., and Lorincz, M.C. (2015). hnRNP K coordinates transcriptional silencing by SETDB1 in embryonic stem cells. PLoS Genet. *11*, e1004933.

Tripathi, V., Sixt, K.M., Gao, S., Xu, X., Huang, J., Weigert, R., Zhou, M., and Zhang, Y.E. (2016). Direct regulation of alternative splicing by SMAD3 through PCBP1 is essential to the tumor-promoting role of TGF-β. Mol. Cell *64*, 549–564.

Villemin, J.-P., Lorenzi, C., Cabrillac, M.-S., Oldfield, A., Ritchie, W., and Luco, R.F. (2021). A cell-to-patient machine learning transfer approach uncovers novel basal-like breast cancer prognostic markers amongst alternative splice variants. BMC Biol. *19*, 70.

Voigt, P., LeRoy, G., Drury, W.J., Zee, B.M., Son, J., Beck, D.B., Young, N.L., Garcia, B.A., and Reinberg, D. (2012). Asymmetrically modified nucleosomes. Cell *151*, 181–193.

Warzecha, C.C., Jiang, P., Amirikian, K., Dittmar, K.A., Lu, H., Shen, S., Guo, W., Xing, Y., and Carstens, R.P. (2010). An ESRP-regulated splicing programme is abrogated during the epithelial-mesenchymal transition. EMBO J. *29*, 3286–3300.

Wei, C., Xiao, R., Chen, L., Cui, H., Zhou, Y., Xue, Y., Hu, J., Zhou, B., Tsutsui, T., Qiu, J., et al. (2016). RBFox2 binds nascent RNA to globally regulate polycomb complex 2 targeting in mammalian genomes. Mol. Cell *62*, 875–889.

Weinert, B.T., Narita, T., Satpathy, S., Srinivasan, B., Hansen, B.K., Schölz, C., Hamilton, W.B., Zucconi, B.E., Wang, W.W., Liu, W.R., et al. (2018). Time-resolved analysis reveals rapid dynamics and broad scope of the CBP/p300 acetylome. Cell *174*, 231–244.e12.

Wenzel, J., Rose, K., Haghighi, E.B., Lamprecht, C., Rauen, G., Freihen, V., Kesselring, R., Boerries, M., and Hecht, A. (2020). Loss of the nuclear Wnt pathway effector TCF7L2 promotes migration and invasion of human colorectal cancer cells. Oncogene *39*, 3893–3909.

Xu, Y., Zhao, W., Olson, S.D., Prabhakara, K.S., and Zhou, X. (2018). Alternative splicing links histone modifications to stem cell fate decision. Genome Biol. *19*, 133.

Yanagisawa, M., Huveldt, D., Kreinest, P., Lohse, C.M., Cheville, J.C., Parker, A.S., Copland, J.A., and Anastasiadis, P.Z. (2008). A p120 catenin isoform switch affects Rho activity, induces tumor cell invasion, and predicts metastatic disease. J. Biol. Chem. *283*, 18344–18354.

Yang, Y., Park, J.W., Bebee, T.W., Warzecha, C.C., Guo, Y., Shang, X., Xing, Y., and Carstens, R.P. (2016). Determination of a comprehensive alternative splicing regulatory network and combinatorial regulation by key factors during the epithelial-to-mesenchymal transition. Mol. Cell Biol. *36*, 1704–1719.

Yearim, A., Gelfman, S., Shayevitch, R., Melcer, S., Glaich, O., Mallm, J.P., Nissim-Rafinia, M., Cohen, A.H., Rippe, K., Meshorer, E., et al. (2015). HP1 is involved in regulating the global impact of DNA methylation on alternative splicing. Cell Rep. *10*, 1122–1134.

STAR★METHODS

KEY RESOURCES TABLE

REAGENT AND RESOURCE	SOURCE	IDENTIFIER
Antibodies		
H3K27me3 ChIP antibody	Cell Signaling	C36B11; RRID:AB_11220433
H3K27Ac ChIP antibody	abcam	ab4729; RRID:AB_2118291
H3K4me1 ChIP antibody	abcam	ab8895; RRID:AB_306847
H3K9Ac ChIP antibody	abcam	ab4441; RRID:AB_2118292
H3K9me2 ChIP antibody	abcam	ab1220; RRID:AB_449854
H3 ChIP antibody	diagenode	C15200011
HA tag ChIP antibody	abcam	ab9110; RRID:AB_307019
total Pol II ChIP antibody	Santa Cruz	sc-55492; RRID:AB_630203
EPCAM-PE FACS antibody	MACS Miltenyi	130-113-264; RRID:AB_2726065
MCAM-APC FACS antibody	MACS Miltenyi	130-120-771; RRID:AB_2752191
CTNND1 e2 FACS antibody	Santa Cruz	sc-23873, RRID:AB_2086394
PE-Cy7 FACS secondary antibody	Thermo Fisher	25-4015-82; RRID:AB_11150243
PTB RNA-IP antibody	Invitrogen	32-4800; RRID:AB_2533082
SUZ12 ChIP antibody	Cell Signaling	D39F6; RRID:AB_2196850
Normal mouse IgG1 control antibody	Invitrogen	14-4714-82; RRID:AB_470111
Chemicals, peptides, and recombinant proteins		
DMEM	Gibco	31966-021
DMEM/F12	Sigma	D8437
EGF	Sigma	E4127
Insulin	Sigma	I5500
Cholera Toxin	Sigma	C8052
L-Glutamine	Sigma	G7513
Hydrocortisone	Sigma	H0888
Penicillin/Streptomycin	Sigma	P4333
CaCl2	Sigma	21115
HEPES Buffered Saline 2X	Sigma	51558
Hygromycin	Invivogen	HGG-40-05
Blasticidin	Invivogen	BLL-40-04
Ampicillin	Sigma	A0166
DRB	Sigma	D1916
TSA	Sigma	T8552
Dynabeads Protein G	Thermo Fisher	10009D
Rnase A	Thermo Fisher	EN0531
Recombinant RNAsin Ribonuclease inhibitor	Promega	N251B
DEPC H2O	BioBasic	DD1005
Glycoblue Coprecipitant	Invitrogen	AM9515
Proteinase K	Thermo Fisher	EO0491
protease Inhibitor	Sigma	11836145001
HEPES	Sigma	H3375
NaCl	Sigma	S5150
EDTA	Invitrogen	15575-038
Glycerol	VWR	24388-295
NP-40/IPEGAL	EMD Millipore	492016
Triton X-100	Sigma	T8787
Tris-HCl pH 8	Sigma	T3038

(*Continued on next page*)

Continued

REAGENT AND RESOURCE	SOURCE	IDENTIFIER
Trizol®	Ambion	15596018
PBS 1X	Sigma	D8537
EGTA	Bio-world	40120128-2
Sodium Deoxycholate	Sigma	D6750
N-lauroylsarcosine	Sigma	L7414
SDS	Biosolve	19812323135
LiCl	Calbiochem	438002
RQ1 Rnase-free Dnase	Promega	#M6101
MNAse	Worthington	LS004797
FGF-2	Sigma	SRP4037
Formaldehyde	Thermo Fisher	28908
ParaFormaldehyde	EMS	15714
Glycine	Sigma	67126
Tween20	Biosolve	20452335
BSA	Sigma	A7906
Crystal Violet	Sigma	61135
Q5 High-Fidelity DNA Polymerase	NEB	M0491
Quick Ligation Kit	NEB	M2200
Q5 Site-Directed Mutagenesis Kit	NEB	E0554
Critical commercial assays		
itaq Universal Syber Green Supermix	Bio-Rad	#1725121
PCR Purification Kit	QIAGEN	28106
GeneJET RNA Purification Kit	Thermo Scientific	#K0732
Transcriptor First Strand cDNA Synthesis Kit	Roche	04 897 030 001
Uncoated Polycarbonate Transwell Chambers	Sigma	CLS3422-48EA
Experimental models: cell lines		
MCF10a cells	Daniel Haber Lab	Javaid et al. (2013)
MCF10a-Snail-ER cells	Daniel Haber Lab	Javaid et al. (2013)
MCF10a-Snail-ER cells - dCas9-empty-GFP	this paper	N/A
MCF10a-Snail-ER cells - dCas9-sid4x-GFP	this paper	N/A
MCF10a-Snail-ER cells - dCas9-p300core-GFP	this paper	N/A
MCF10a-Snail-ER cells - dCas9-EZH2core-GFP	this paper	N/A
MCF10a-Snail-ER cells - dCas9-vSETx2-GFP	this paper	N/A
MCF10a-Snail-ER cells - dCas9-UTXcore-GFP	this paper	N/A
HEK293T	ATCC	CRL-3216
Oligonucleotides		
ChIP-qPCR primers	this paper	Table S1
RT-qPCR primers	this paper	Table S1
Pol II measurement primers	this paper	Table S1
RIP-qPCR primers	this paper	Table S1
MNAse-qPCR primers	this paper	Table S1
cloning gRNAs	this paper	Table S1
cloning shRNAs	this paper	Table S1
cloning and mutagenesis of dCas9 fusion primers	this paper	Table S1
Recombinant DNA		
psPAX2	Addgene	12260
pMD2.G	Addgene	12259
dCas9-VP64-GFP	Addgene	61422

(*Continued on next page*)

Continued

REAGENT AND RESOURCE	SOURCE	IDENTIFIER
dCas9-empty-GFP	this paper	N/A
pAC94-sid4x	Maayan Salton Lab	N/A
dCas9-sid4x-GFP	this paper	N/A
dCas9-p300core*-GFP	this paper	N/A
pcDNA-dCas9-p300 Core	Addgene	61357
dCas9-p300core-GFP	this paper	N/A
dCas9-vSETx2*-GFP	this paper	N/A
pAC154-dual-dCas9-2xvSET	Philipp Voigt Lab	N/A
dCas9-vSETx2-GFP	this paper	N/A
pEBB-EZH2-FLAG	Colin Ducket Lab	(Hwang et al., 2008)
dCas9-hEZH2core-GFP	this paper	N/A
pCS2-UTX-F	Kai Ge Lab	Hong et al. (2007)
dCas9-UTXcore-GFP	this paper	N/A
pKLV2.2-h7SKgRNA5(SapI)-hU6gRNA5(BbsI)-PGKpuroBFP-W	Addgene	72666
pKLV2.3-Hygro	this paper	N/A
pKLV2.3-Hygro + gRNAs	this paper	Table S1
pLKO.1-Hygro	Addgene	24150
pLKO.1-Blast	Addgene	26655
pLKO.1-Hygro or Blast + shRNAs		
Software and algorithms		
MRI Wound healing Tool	Volker Baecker, Montpellier RIO Imaging	http://dev.mri.cnrs.fr/projects/imagej-macros/wiki/Wound_Healing_Tool
Flowing Software	Perttu Terho, Turku Centre for Biotechnology	http://flowingsoftware.btk.fi/
BD FACS Chorus	BD Biosciences - US	https://www.bdbiosciences.com/us/instruments/research/software/flow-cytometry-acquisition/bd-facschorus-software/m/6729689/resources
RBPDB v1.3	University of Toronto - Canada	http://rbpdb.ccbr.utoronto.ca
RBPMAP v1.1	Mandel-Gutfreund lab	http://rbpmap.technion.ac.il
SFMAP v1.8	Mandel-Gutfreund lab	http://sfmap.technion.ac.il/
Spliceaid	Polytechnic University or Marche - Italy	http://www.introni.it/splicing.html
catRAPID	CRG Technology & Business Development Office	http://s.tartaglialab.com

RESOURCE AVAILABILITY

Lead contact

Further information and requests for resources and reagents should be directed to and will be fulfilled by the lead contact, Reini F. Luco (reini.luco@igh.cnrs.fr).

Materials availability

Plasmids generated in this study can be obtained upon request.

Data and code availability

- All data reported in this paper will be shared by the lead contact upon request.
- This paper does not report original code.
- Any additional information required to reanalyze the data reported in this paper is available from the lead contact upon request.

EXPERIMENTAL MODEL AND SUBJECT DETAILS

Cell lines and cell culture

MCF10a cells

MCF10a cells are non-transformed human female breast epithelial cells. MCF10a-Snail-ER cell line was generated by introducing a Snail-1 retroviral expression construct using a fused estrogen receptor (ER) response element to mediate regulation by exogenous 4-hydroxy-tamoxifen (4-OHT) and was obtained from Daniel A. Haber lab with its parental cell line (Javaid et al., 2013). All MCF10a cell lines were maintained at 37°C with 5% CO_2 in DMEM/F12 supplemented with 5% horse serum, 10 ng/mL EGF, 10 μg/mL insulin, 0.1 μg/mL cholera toxin, 0.5 μg/mL hydrocortisone, 1% penicillin/streptomycin, 1% L-glutamine (complete medium).

EMT induction and MET

MCF10a-Snail-ER cells were seeded at 7.5 × 10^5 cells/150 mm dish in complete medium (DMEM/F12 supplemented with 10 ng/mL EGF, 10 μg/mL insulin, 0.1 μg/mL cholera toxin, 0.5 μg/mL hydrocortisone, 1% w/v penicillin/streptomycin and 5% of Horse Serum). 24 h hours after plating, cells were synchronized by replacing cell media with a No serum medium (same composition than complete medium except for 0% of Horse Serum) for 15 h. Cells were then cultured back in complete medium with 100 nM 4-hydroxy-tamoxifen (4-OHT) for EMT reprogramming, or Methanol (which is the control vehicle) for untreated conditions (UNT) until the indicated time point (T0.25, T0.5, T1, T7).

MET was obtained by plating 1.25 × 10^6 EMT-induced cells/150 mm dishes in MCF10a media without tamoxifen and passing them each 7 days at the same concentration as seeded (1.25 × 10^6 cells/150 mm dishes). It takes 21 days to completely reverse the MET, which is the moment the cells were collected for analysis.

HEK293T cells

HEK293T were maintained at 37°C with 5% CO_2 in DMEM supplemented with 10% fetal bovine serum, 1% penicillin/streptomycin, 1% L-glutamine. HEK293T are transfected by Calcium Phosphate transfection to generate recombinant lentiviruses.

Cloning and plasmids

To generate plasmid DNAs encoding GFP/HAtag epitope-tagged sid4x (a gift from Salton lab), p300core (addgene 61357), EZH2core (a gift from Ducket lab), vSETx2 (from Voigt lab) and UTX core (a gift from Ge lab), the cDNAs were amplified using Q5 High-Fidelity DNA Polymerase (NEB) with primers carrying the appropriate restriction enzymes sites AscI/SbfI (See Table S1 for the list of primers used) and cloned using Quick DNA Ligation Kit (NEB) into dCas9-empty-GFP vector. dCas9-empty-GFP vector has been generated by cutting dCas9-VP64-GFP plasmid (addgene 61422) by BamHI and NheI restriction enzymes to remove VP64 sequence, followed by introduction of a linker containing AscI and SbfI restriction sites and a HAtag epitope-tagged. Q5 Site-Directed Mutagenesis Kit (NEB) was used for generating dCas9 plasmids encoding the mutant p300core* (Y1467F) and vSETx2* (Y105F x2) proteins. Mutagenesis primer sequences and plasmids used in this study are listed in Table S1. To generate pKLV2.3-Hygro gRNA lentiviral plasmid, the commercial pKLV2.2-PGKpuroBFP plasmid (addgene 72666) was modified by removing the puromycin resistance and the BFP tag, an EcoRI site was added and hygromycin resistance was introduced in XhoI/EcoRI restriction sites. The different gRNAs were cloned by using SapI or BbsI restriction sites. Cloning primer sequences and gRNAs used in this study are listed in Table S1. shRNA plasmids were gifts from different laboratories (See Table S1) or obtained by cloning shRNA sequences into pLKO.1-Hygro (addgene 24150) or pLKO.1-Blast (addgene 26655) plasmids with AgeI/EcoRI restriction sites. shRNA sequences used in this study are listed in the Table S1.

Expression and purification of vSET constructs

The coding sequence fo vSET was ordered from IDT and cloned into a modified pET22b plasmid. Single-chain dimeric vSET constructs with GSGSG-(SSG)n-SGSGG linkers (n = 1–3) in between two vSET monomers were generated by PCR and subcloning of a fragment encoding the C-terminal 8 residues of vSET followed by the linker and a complete vSET monomer into the XbaI and HindIII restriction sites of vSET in modified pET22b.

vSET and dimeric sc-vSET (called vSETx2 in this paper) constructs were expressed in BL21 *E. coli* and purified from inclusion bodies essentially as described for vSET by (Manzur et al., 2003). In short, inclusion bodies were solubilized in unfolding buffer (20 mM Tris pH 7.5, 7 M guanidine hydrochloride, 10 mM DTT). To refold vSET and vSETx2 proteins, solubilized protein was first dialyzed against urea dialysis buffer (10 mM Tris pH 7.5, 7 M urea, 100 mM NaCl, 1 mM EDTA, 5 mM ß-mercaptoethanol), followed by repeated dilution with vSET refolding buffer (50 mM Tris pH 7.5, 300 mM NaCl, 10% glycerol, 0.1 mM EDTA, 5 mM ß-mercaptoethanol) reducing the concentration of urea from 7 M to 1 M in a step-wise fashion in increments of 1 M (1 h/dialysis step). Finally, refolded vSET and vSETx2 proteins were dialyzed once against vSET refolding buffer and then once against vSET HEPES refolding buffer (50 mM HEPES pH 7.5, 300 mM NaCl, 5% glycerol, 0.1 mM EDTA, 5 mM ß-mercaptoethanol).

Size exclusion chromatography of refolded vSET and vSETx2 constructs was performed on a Superdex 75 column in vSET HEPES refolding buffer.

vSETx2 construct specificity towards H3K27 was tested by methyltransferase assays in which the substrate nucleosomes were harbouring an H3K27A mutation (Figure S3B).

METHOD DETAILS

Methyltransferase assays

In vitro histone methyltransferase (HMT) assays were carried out essentially as described in (Voigt et al., 2012). Briefly, core histones were expressed in E. coli, purified from inclusion bodies and assembled into histone octamers by dialysis into refolding buffer (10 mM Tris pH 8, 2 M NaCl, 1 mM EDTA, 5 mM ß-mercaptoethanol). Correctly assembled octamers were purified by size exclusion chromatography on a Superdex S200 column. Recombinant nucleosome arrays were reconstituted via salt dialysis assembly of histone octamers onto plasmid DNA containing 12 177-bp repeats of the 601 nucleosome positioning sequence. To determine methylation activity, 2–10 ng of vSET or VSETx2 constructs were incubated with 1 μg of recombinant nucleosome arrays in 50 mM Tris pH 8.5, 5 mM $MgCl_2$, 4 mM DTT, and ^{3}H-labeled SAM for 1 h at 30°C. Reactions were stopped by addition of SDS loading buffer. After separation by SDS-PAGE and transfer to PVDF membranes, loading was assessed by Coomassie staining. Activity was detected as incorporation of ^{3}H via exposure of Biomax MS film with the help of Biomax Transcreen LE (both Kodak Carestream) intensifying screens.

Epigenome editing

Stable cell lines of MCF10a-Snail-ER expressing the different dCas9s were generated. Briefly, cells were infected with recombinant viruses containing dCas9-empty-GFP, dCas9-sid4x-GFP, dCas9-p300core-GFP, dCas9-EZH2core-GFP, dCas9-vSETx2-GFP or dCas9-UTXcore-GFP following Recombinant Lentivirus Production protocol. Infected cells were harvested and GFP-sorted using a BD FACS Melody (BD Biosciences-US). GFP was excited by a 488-nm laser line and its emission was collected through 527/32BD. dCas9 Stable cell lines were then infected with Lentiviruses containing pKLV2.3-Hygro + gRNAs, were split and medium was supplemented with 100 μg/mL hygromycin. See Table S1 for the list of gRNAs used.

Recombinant lentivirus production

HEK393T were split at 2 × 10^6 cells/100 mm dish (Day 1). Cells were transfected with 1 μg psPAX2 plasmid (VSVG env gene), 1 μg pMD2.G plasmid (gag, pol, and accessory proteins), 5 μg of plasmid of interest (eg. dCas9-empty), 250 mM $Cacl_2$, qsp 500 μL sterile water. Samples were gently mixed and completed with 2X HEPES Buffered Saline (HBS), Incubated 15 min at room temperature. Mixes were dropped on HEK293T and cells were maintained at 37°C with 5% CO_2 (Day 2). 15 h after transfection medium was replaced by MCF10a complete medium and MCF10a cells were split at 5 × 10^5 cells/100 mm dish for further infections (Day 3). 48 h and 72 h after transfection, viruses were collected, filtered through 0.45 μm filter, and dropped on MCF10a cells (Days 4 and 5). 72 h after, cells were split and medium was supplemented with 15 μg/mL blasticidin or 100 μg/mL hygromycin.

Chromatin immunoprecipitation

We performed ChIP using H3K27me3 antibody (Cell Signaling C36B11), H3K27Ac antibody (abcam 4729), H3K4me1 antibody (abcam 8895), H3K9Ac antibody (abcam 4441), H3K9me2 antibody (abcam 1220), H3 antibody (Diagenode C15200011), HAtag antibody (abcam 9110), SUZ12 (Cell Signaling 3737S), total Pol-II antibody (Santa Cruz sc-55492). MCF10a cells (10 million per sample) were fixed in 1% formaldehyde in PBS at room temperature with agitation for 2 min (Histone marks), 4 min (HAtag), 10 min (Total Pol-II), then quenched with 1M glycine for 5 min. Fixed cells were resuspended in 1 mL cold Lysis Buffer A (50 mM HEPES pH 7.5, 140 mM NaCl, 1 mM EDTA, 10% glycerol, 0.5% NP-40/Igepal, 0.25% Triton X-100) prepared fresh with protease inhibitors (Sigma 11836145001) and incubated at 4°C on rotating wheel for 10 min. Nuclei were pelleted and resuspended in 1 mL Lysis Buffer B (10 mM Tris-HCl pH 8, 200 mM NaCl, 1 mM EDTA, 0.5 mM EGTA, prepared fresh with protease inhibitors), and incubated on rotating wheel for 10 min. Samples were then diluted with 0.75 mL Dilution Buffer C (10 mM Tris-HCl pH 8, 100 mM NaCl, 1 mM EDTA, 0.5 mM EGTA, 0.1% sodium deoxycholate, 0.5% N-lauroylsarcosine, prepared fresh with protease inhibitors), and sonicated at 4°C for 12, 14, 16 min (for 2, 4, 10 min cross-linking respectively) to generate fragments from 200 bp to 1kp long. After sonication, samples were spun at 20,000xg for 30 min at 4°C to remove debris. 8 μg (Histone marks, HAtag) or 25 μg (Total Pol-II) of chromatin were diluted in TSE 150 Buffer (0.1% SDS, 1% Triton X-100, 2 mM EDTA, 20 mM Tris-HCl pH 8, 150 mM NaCl, supplemented with protease inhibitors) and cleaned-up with 30 μL of pre-washed Dynabeads Protein G (Thermo Fisher 10009D) and incubated at 4°C on rotating wheel for 1h30. Prior to setting up immunoprecipitation ("IP") reactions, 50 μL of precleared chromatin was removed as "Input." 150 μL of TE/1% SDS Buffer (10 mM Tris-HCl pH 8, 1 mM EDTA pH 8, 1% SDS) was added to "Input" and incubated overnight at 65°C. 3 μL of proteinase K (Thermo Fisher EO0491) was added and samples were incubated at 37°C for 2 h. Following the incubation, "Input" DNA was purified using the QIAquick PCR Purification kit (QIAGEN 28106) per the manufacturer's instructions. To set up IP reactions, precleared chromatin was mixed with antibody and rotated overnight at 4C. IP reactions was added to 30 μL pre-washed Dynabeads Protein G and rotated 1h30 at 4°C. Beads were washed once with TSE 150 Buffer, once with TSE 500 Buffer (0.1% SDS, 1% Triton X-100, 2 m M EDTA, 20 mM Tris-HCl pH 8, 500 mM NaCl), once with Washing Buffer (10 mM Tris-HCl pH 8, 1 mM EDTA, 0.25 M LiCl, 0.5% NP-40/Igepal, 0.5% sodium deoxycholate), and twice with TE (10 mM Tris-HCl pH 8, 1 mM EDTA pH 8). Following the final wash, beads were eluted with 100 μL of Elution Buffer (50 mM Tris-HCl pH 8, 10 mM EDTA, 1% SDS) 15 min at 65°C while vigorously shaking, and 100 μL of TE/1% SDS Buffer for a final eluate volume of 200ul. The following were incubated overnight at 65°C. 3 μL of proteinase K was added and samples were incubated at 37°C for 2 h. Following the incubation, DNA was purified using the QIAquick PCR Purification kit (QIAGEN 28106) per the manufacturer's instructions. Input and immunoprecipitated DNA were then analyzed by

QPCR using the iTaq Universal Syber Green supermix (Bio-Rad #1725121) on the Bio-Rad CFX-96 Touch Real-Time PCR System. Results are represented as the mean value +/− S.E.M of at least 3 independent experiments of immunoprecipitated chromatin (calculated as a percentage of the input) after normalization by the mean of two control regions stably enriched across the different conditions. See Table S1 for the list of gene-specific primers used.

RNA extraction and RT-qPCR

Quantitative RT-PCR analysis was performed in biological triplicates or quadruplicates. Total RNAs were prepared from cells with the GeneJET RNA Purification Kit (Thermo Scientific #K0732). All samples were eluted into 30 μL RNAse-free water. DNAs was remove from RNA by using RQ1 RNase-Free DNase (Promega #M6101), briefly, 1 μg of RNA was mixed with RQ1 DNase and RQ1 DNase 10X Reaction Buffer and incubated 30 min at 37°C. RQ1 enzyme was inactivated by adding Stop Solution 10 min at 65°C. cDNAs were generated using the Transcriptor First Strand cDNA Synthesis kit (Roche 04 897 030 001) according to the manufacturer's instructions. For each biological replicate, quantitative PCR reactions were performed in technical duplicates using the iTaq Universal Syber Green supermix (Bio-Rad) on the Bio-Rad CFX-96 Touch Real-Time PCR System, and the data normalized to TBP. Data from biological replicates are plotted as mean ± S.E.M. See Table S1 for the list of gene-specific primers used.

Migration and invasion assays

Non-directional migration - wound healing assay

MCF10a cells were plated at 1 × 10^6 cells/well in 6 well plates containing complete medium and they were grown to confluency. Confluent cultures were serum-starved for 12 hours. Serum-starved, confluent cell monolayers were wounded with a plastic pipette tip and they were washed three times with PBS to remove floating cells. Following washing, the cells were cultured in complete medium. The wounded area was photographed at 0 h (control) and 24 hours later using a Zeiss axiovert 40 CFL microscope with a 10X objective (100X magnification). Cell migration into the scratch was quantified using ImageJ plugin MRI Wound Healing Tool (Volker Baecker, Montpellier RIO Imaging).

Directional migration – transwell filter assay

Cell migration assay was performed using 24 well chambers (Sigma CLS3422-48EA) with uncoated polycarbonate membranes (pore size 8 μm). Briefly, 5 × 10^4 cells resuspended in depleted medium (DMEM/F12 supplemented with 1% horse serum, 10 μg/mL insulin, 0.1 μg/mL cholera toxin, 0.5 μg/mL hydrocortisone, 1% penicillin/streptomycin, 1% L-glutamine) were placed in the upper chamber of the transwell unit. The bottom chamber was filled with 0.6 mL complete medium supplemented with 20 ng/mL FGF-2. The plates were incubated for 12 h at 37°C with 5% CO_2 and the cells migrating from the upper to the lower chamber of the unit were fixed with 4% paraformaldehyde in PBS 2 min, permeabilized with 0.1% Triton X-100 for 5 min and stained with 0.2% crystal violet for 1 h. Migrating cells were counted using a Zeiss axiovert 40 CFL microscope with a 5X objective (50X magnification).

Invasion – transwell filter assay

For cell invasion assay, 24 well chambers were coated with Matrigel (Sigma E6909) diluted in depleted medium for 1 h at 37°C and assays were performed as described in Directional migration except the assay was performed for 24 h.

Flow cytometry

MCF10a cells were fixed in 4% Paraformaldehyde for 10 min at room temperature followed by a 15 min permeabilization step in 0.5% Tween20. Cells were resuspended in Blocking Buffer (PBS, 3% BSA, 0.1% Tween20) for 30 min on rotating wheel at room temperature and incubated with conjugated antibodies EPCAM-PE (MACS Miltenyi 130-113-264) and MCAM-APC (MACS Miltenyi 130-120-771) for 1h30 on rotating wheel at room temperature protected from light. Cells were harvested and analyzed using a MACS Quant 10 (MACS Miltenyi Biotec). PE was excited by a 488-nm laser line (laser DPSS) and its emission was collected through 655/605 nm; APC was excited by a 640-nm laser line and its emission was collected through 655/730 nm. The data were analyzed using Flowing software (Perttu Terho, Turku Centre for Biotechnology).

Cell sorting - FACS

Cells were resuspended in Blocking Buffer (PBS, 3% BSA) for 30 min on rotating wheel at room temperature and successively incubated with CTNND1 exon 2 primary antibody (Santa Cruz sc-23873) for 1h30 on rotating wheel at room temperature, and PE-Cy7 secondary antibody (Thermo Fisher 25-4015-82) for 30 min on rotating wheel at room temperature protected from light. Cells were harvested and analyzed using a BD FACS Melody (BD Biosciences-US). PE-Cy7 was excited by a 561-nm laser line and its emission was collected through 783/56BD. The data were analyzed using BD FACS Chorus software (BD Biosciences-US) and only cells with protein levels above the no primary antibody background signal were collected.

Polymerase II elongation measurement

A DRB treatment (Sigma D1916) of 100 μM for 6 h was necessary in order to fully block endogenous CFTR transcription. Cells were washed and the kinetic (0, 5, 10, 15, 20, 30, 45, 60, 90 min) was started by adding complete medium. For each time point of the kinetic, cells are scraped and cell pellets are snap frozen in liquid nitrogen. Total RNA was extracted as mentioned above in RNA Extraction and RT-qPCR. Reverse transcriptase reaction was initiated with random hexamers. Quantification of the pre-mRNAs was performed by real-time PCR with amplicons spanning the intron-exon junctions. For each biological replicate, quantitative PCR reactions were

performed in technical duplicates using the iTaq Universal Syber Green supermix (Bio-Rad) on the Bio-Rad CFX-96 Touch Real-Time PCR System, and the data normalized by tRNA. Data from biological replicates are plotted as mean ± S.E.M. See Table S1 for the list of gene-specific primers used.

TSA, panobinostat and DRB treatments

A 24 hours treatment of 40 μM of DRB (Sigma D1916) or 1 μg/mL of TSA (Trichostatin A – Sigma T8552) was applied on MCF10a-Snail-ER cells after 0 days (T0) or 7 days (T7) of EMT induction, to impede the dynamics of transcribing RNA Polymerase II. Total RNA extraction and quantification were performed as mentioned above in Polymerase II Elongation measurement.

For HDAC inhibition during EMT reprogramming, MCF10a-Snail-ER cells were treated with 3 μg/mL of TSA (Trichostatin A – Sigma T8552) or 10 nM of Panobinostat (gift from Moreaux Lab, IGH - Ha et al., 2014) at the same time as addition of Tamoxifen for EMT induction during 24 h.

MNase protection assay for nucleosome positioning

6×10^6 cells per condition were cross-linked with formaldehyde for 1 min as in the ChIP protocol. Then, cells were lysed using RSB buffer (NaCl 10 mM, MgCl2 5 mM, Tris 10 mM pH 7.5) for 10 min in ice. IGEPAL and NP-40 were added to 0.5% final concentration each and cells were dounced 10 times. The number of nuclei were counted using trypan blue, and after 5 min of refrigerated centrifugation at 2500 rpm, 5×10^6 nuclei were resuspended in 400 μL of digestion buffer (NaCl 15 mM, CaCl2 1 mM, KCl 60 mM, Tris 15 nM pH 8, Sucrose 250 mM and fresh DTT 0.5 mM). Samples were split in 2. 200 μL were stored at −80°C and the rest were diluted with an equal volume (200 μL) of digestion buffer for a 5 min incubation with 15 U MNAse per sample at 37°C. The reaction was stopped by adding 400 μL of stop solution (100 mM $NaHCO_3$, 20 mM EDTA and 1% SDS) and 90 min incubation at 65°C. Finally, the samples were treated for 30 min with 5 μL RNAse A (1 mg/mL) at 37°C, followed by 3 μL of Proteinase K for 12 h at 65°C. Next day, DNA was extracted using phenol:chloroform and protected DNA was quantified using qPCR as described. The primers used are listed in the Table S1.

shRNA knock-down

Knock-down of HDAC1, HDAC2, PTB, ELAV1, ESRP1, MBNL1, hnRNPFH1, CELF1, hnRNPF, SRSF1, FUS, RBFOX2, SOX9, SMAD3 and PCBP1 was performed according to the Recombinant Lentivirus Production protocol. Briefly, HEK293T cells were transfected with the appropriate shRNA plasmid, 15 h after transfection medium was replaced by MCF10a complete medium and MCF10a cells were split for further infections. 48 h and 72 h after transfection, viruses were collected, filtered through 0.45 μm filter, and dropped on MCF10a cells. 72 h after, cells were split and medium was supplemented with 15 μg/mL blasticidin or 100 μg/mL hygromycin.

In the case of the double HDAC1+2 knock-down, cells were infected first with the shRNA against HDAC1, selected using blasticidin, and then infected with a second virus containing the shRNA against HDAC2. After 72 h of hygromycin selection, double infected cells were EMT induced with tamoxifen for 24 h.

A non-mammalian targeting shRNA was used as a negative control.

UV cross-linked RNA-immunoprecipitation

The day before collection, 10^7 cells were seeded per condition and IP reaction (5×10^6 for PTB and 5×10^6 for normal mouse IgG1 IP's) in a p15 plate. Next, day, cell media was discarded and each plate was washed with 12 mL of cold PBS 1X (D8537, Sigma-Aldrich). Cells were UV-crosslinked at 254 nm with 2000 J/m^2 in ice and scrapped. After centrifugation at 2500 rpm for 5 min, the PBS was discarded and the pellets were stored at −80°C until processing. Cells were lysed in 617.5 μL of cell lysis buffer (1% v/v NP-40, 400 U/mL of RNAse inhibitor in 1x PBS) for 10 min in ice. Sodium deoxycholate was added to 0.5% v/v final concentration and samples were incubated with rotation for 15 min at 4°C. Samples were incubated at 37°C with 30 U of DNAse with shacking at 300 rpm, vortexed briefly and sonicated for 10 cycles x (30″ on/30″ off, high setting condition) in 15 mL conical polystyrene tubes using a Bioruptor™ (Diagenode) sonicator with a 4°C water bath cold circulation system. After that, the tubes were spun to recover all sample and centrifuged for 15 min at 21,130 rcf to remove insoluble debris. Every sample was divided in 2 × 300 μL aliquots and 30 μL were saved as « Input » control and stored at −80°C. Every aliquot was incubated with 6 μg of α-PTB (Ref. 32-4800, Invitrogen) or 6 μg of α-normal mouse control IgG1 (Ref. 14-4714-82, Invitrogen), o/n with rotation at 4°C. Next day, 40 μL of Dynabeads protein G (Ref. 10009D, Invitrogen), pre-washed three times with 1 mL 1xPBS 0.01% v/v Tween-20, were added per sample and incubated for 4 h at 4°C with rotation. The unbound supernatant was discarded and beads were washed once with Cell Lysis Buffer (1% v/v NP-40, 0.5% sodium deoxycholate in 1X PBS), three times with Washing Buffer I (1% v/v NP-40, 0.5% sodium deoxycholate, 300 mM NaCl in 1X PBS), once with Washing Buffer II (0.5% v/v NP-40, 0.5% sodium deoxycholate, 0.125% v/v SDS in 1X PBS) and once in PBS 1X. All washes were done for 5 min with rotation at 4°C. Beads and Inputs were incubated with 100 μL of Proteinase K buffer (100 mM Tris-HCl pH 8, 50 mM NaCl, 10 mM EDTA, 0.5% v/v SDS, 100 U RNAsin of in DEPC water) and 10 μL of Proteinase K for 45 min at 25°C shacking at 1,500 rpm. 1 mL of Trizol® (Ambion) was added per sample (beads or input) and RNA was purified according to manufacturer's protocol, including 1 μL of Glycoblue™ Coprecipitant (Ref. AM9515, Invitrogen). RNA pellets were resuspended in 8 μL of DEPC water and incubated with μl (1U DNAse) and 1 μL of 10X DNAse buffer (Ref. M6101, Promega) for 30 min at 37°C. The DNAse was inactivated with 1 μL of Stop Solution at 65°C for 10 min and RT was performed using Transcriptor First Strand cDNA Synthesis Kit (Ref. 04 897 030 001, Roche) in a final volume of 20 μL. RT was diluted 1/5 and each sample was quantified

in duplicates as described before using the primers listed in Table S1. The enrichment of every IP was normalized to its Input using (2^(Ct IP-Ct Input) and for representation the fold change was calculated relative to IgG enrichment.

RNA motif search analysis

RNA binding motif search analysis was done using CTNND1 exon2 sequence in four public softwares: RBPDB v1.3 (http://rbpdb.ccbr.utoronto.ca), RBPMAP v1.1 (http://rbpmap.technion.ac.il), SFMAP v1.8 (http://sfmap.technion.ac.il/), Spliceaid (http://www.introni.it/splicing.html). All softwares were used with the default parameter settings, except for some exceptions. For RBPDB the threshold 0.8 was applied. For RBPMAP, the Stringency level used was ''High stringency'' with all motifs available from Human/mouse. For SFMAP both ''Perfect match'' and ''High stringency'' stringency levels were used. For catRAPID, the following settings were used: ''Full-length proteins'', ''RNA and DNA binding'' and including ''disordered proteins. We prioritized the RNA motifs predicted by more than one database and expressed in MCF10a cells.

QUANTIFICATION AND STATISTICAL ANALYSIS

All results are represented as mean ± SEM. The exact number of biological replicates (n) used in each experiment is indicated in the corresponding figure legend. We used as statistical analysis the two-tailed paired Student's t-test with two-sample unequal variance (heteroscedastic) calculated in Microsoft Excel (version 2112). Only significant p-values are represented using the following asterisks code, *P < 0.05, **P < 0.01, ***P < 0.00, as indicated in figure legends.

Cell Reports, Volume *38*

Supplemental information

Histone marks regulate the epithelial-to-mesenchymal transition via alternative splicing

Alexandre Segelle, Yaiza Núñez-Álvarez, Andrew J. Oldfield, Kimberly M. Webb, Philipp Voigt, and Reini F. Luco

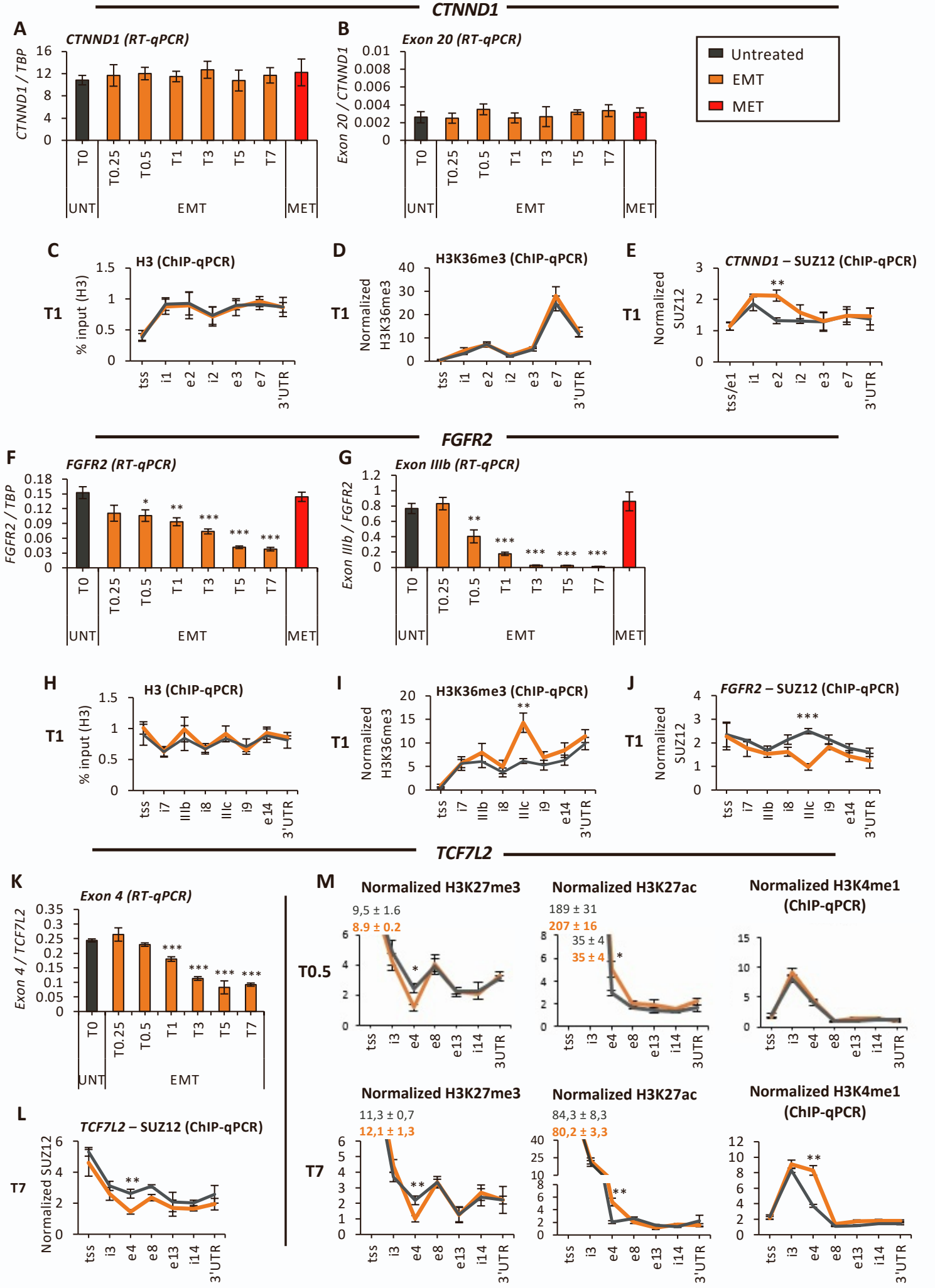
CTNND1
A
CTNND1 (RT-qPCR)
CTNND1 / TBP
B
Exon 20 (RT-qPCR)
Exon 20 / CTNND1
Untreated
EMT
MET
T0
T0.25
T0.5
T1
T3
T5
T7
UNT
EMT
MET
C
H3 (ChIP-qPCR)
% input (H3)
D
H3K36me3 (ChIP-qPCR)
Normalized H3K36me3
E
CTNND1 – SUZ12 (ChIP-qPCR)
Normalized SUZ12
T1
tss
i1
e2
i2
e3
e7
3'UTR
FGFR2
F
FGFR2 (RT-qPCR)
FGFR2 / TBP
G
Exon IIIb (RT-qPCR)
Exon IIIb / FGFR2
H
H3 (ChIP-qPCR)
I
H3K36me3 (ChIP-qPCR)
J
FGFR2 – SUZ12 (ChIP-qPCR)
i7
IIIb
i8
IIIc
i9
e14
TCF7L2
K
Exon 4 (RT-qPCR)
Exon 4 / TCF7L2
L
TCF7L2 – SUZ12 (ChIP-qPCR)
T7
M
Normalized H3K27me3
Normalized H3K27ac
Normalized H3K4me1 (ChIP-qPCR)
T0.5
9,5 ± 1.6
8.9 ± 0.2
189 ± 31
207 ± 16
35 ± 4
35 ± 4
11,3 ± 0,7
12,1 ± 1,3
84,3 ± 8,3
80,2 ± 3,3
e4
e8
e13
i14
3UTR

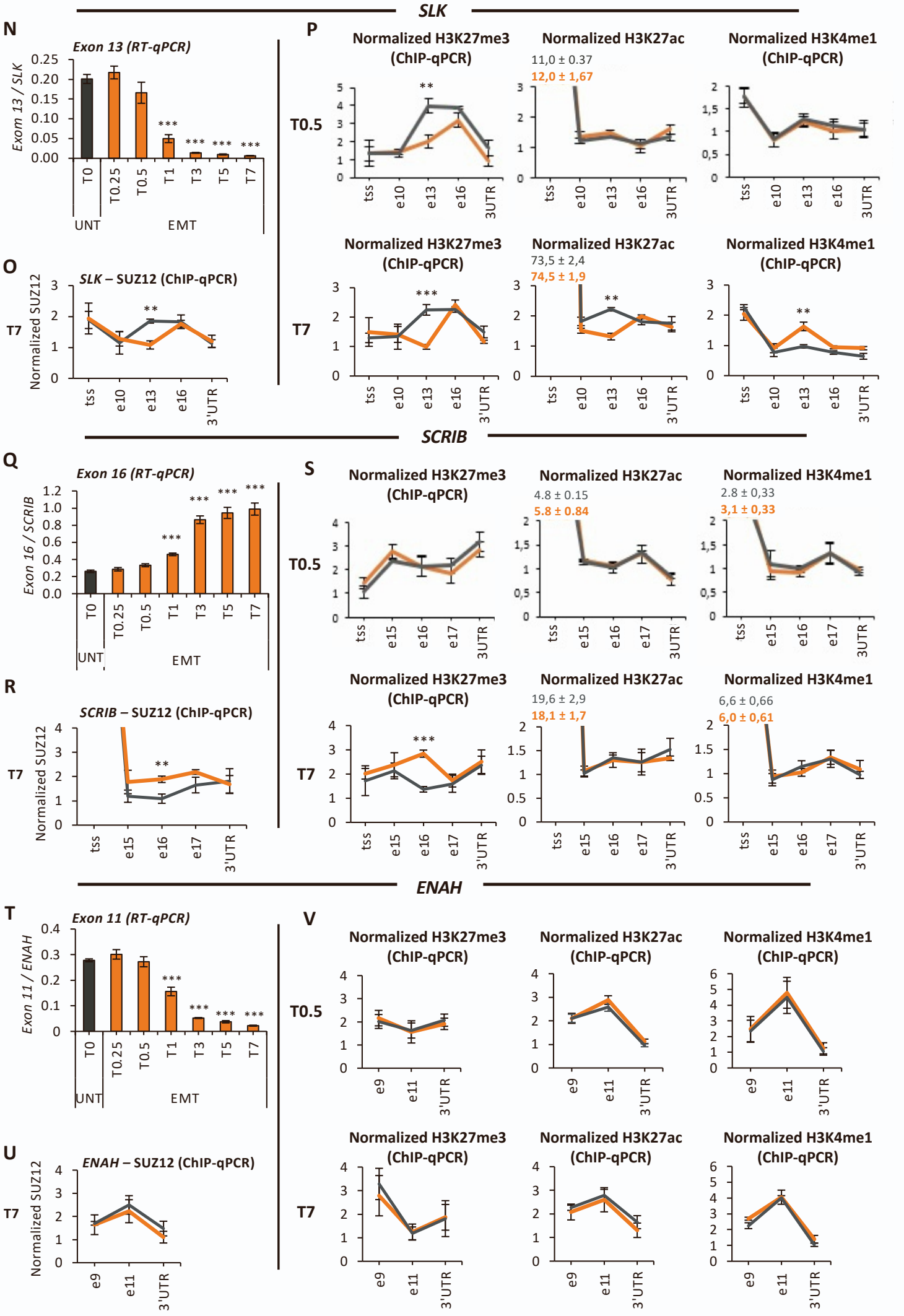
SLK
N
Exon 13 (RT-qPCR)
Exom 13 / SLK
0.25
0.20
0.15
0.10
0.05
0.00
***
T0
T0.25
T0.5
T1
T3
T5
T7
UNT
EMT
O
SLK – SUZ12 (ChIP-qPCR)
T7
Normalized SUZ12
**
tss
e10
e13
e16
3'UTR
P
Normalized H3K27me3 (ChIP-qPCR)
Normalized H3K27ac
11,0 ± 0.37
12,0 ± 1,67
Normalized H3K4me1 (ChIP-qPCR)
T0.5
T7
73,5 ± 2,4
74,5 ± 1,9
SCRIB
Q
Exon 16 (RT-qPCR)
Exon 16 / SCRIB
1.2
1.0
0.8
0.6
0.4
0.2
0.0
R
SCRIB – SUZ12 (ChIP-qPCR)
e15
e16
e17
S
4.8 ± 0.15
5.8 ± 0.84
2.8 ± 0,33
3,1 ± 0,33
19,6 ± 2,9
18,1 ± 1,7
6,6 ± 0,66
6,0 ± 0,61
ENAH
T
Exon 11 (RT-qPCR)
Exon 11 / ENAH
0.4
0.3
0.2
0.1
0
U
ENAH – SUZ12 (ChIP-qPCR)
e9
e11
V

Figure S1. Localised enrichment of specific histone marks at alternatively spliced exons during EMT, related to Figure 1 and 2: (**A,B**) *CTNND1* and exon 20 expression levels relative to total *TBP* and *CTNND1*, respectively, during EMT and MET in tamoxifen-induced MCF10a-Snail-ER cells by RT-qPCR (mean +/- SEM, n=4). (**C,D,E**) Enrichment levels of H3, H3K36me3 and SUZ12 along *CTNND1* locus in tamoxifen-induced MCF10a-Snail-ER cells for 24h by ChIP-qPCR (mean +/- SEM, n=4). H3 enrichment levels are represented as percentage of input. For H3K36me3 and SUZ12, the percentage of input was normalized by two control regions across the different conditions. (**F,G**) *FGFR2* and exon IIIb expression levels relative to total *TBP* and *FGFR2*, respectively, during EMT and MET in tamoxifen-induced MCF10a-Snail-ER cells by RT-qPCR (mean +/- SEM, n=4). (**H,I,J**) Enrichment levels of total H3, H3K36me3 and SUZ12 along *FGFR2* locus in tamoxifen-induced MCF10a-Snail-ER cells for 24h by ChIP-qPCR (mean +/- SEM, n=4 H3 enrichment levels are represented as percentage of input. For H3K36me3 and SUZ12, the percentage of input was normalized by two control regions across the different conditions. (**K,N,Q,T**) Inclusion levels of alternatively spliced exons essential for EMT: *TCF7L2* exon 4 (K), *SLK* exon 13 (N), *SCRIB* exon 16 (Q) and *ENAH* exon 11 (T) in MCF10a-Snail-ER during induction of EMT and reversible MET. RT-qPCR values were normalized by total expression levels of *SLK*, *TCF7L2*, *SCRIB* and *ENAH*, respectively (mean +/- SEM, n=4). (**L,O,R,U**) Enrichment levels of SUZ12 along *TCF7L2* (**L**), *SLK* (**O**), *SCRIB* (**R**) and *ENAH* (**U**) in tamoxifen-induced MCF10a-Snail-ER cells for 7 days (T7) by ChIP-qPCR (mean +/- SEM, n=4). (**M,P,S,V**) Enrichment levels of H3K27me3, H3K27ac and H3K4me1 along *TCF7L2* (**M**), *SLK* (**P**), *SCRIB* (**S**) and *ENAH* (**V**) in tamoxifen-induced MCF10a-Snail-ER cells for 12h (T0.5) or 7 (T7) days by ChIP-qPCR (mean +/- SEM, n=4). The percentage of input was normalized by two control regions across the different conditions. *P <0.05, **P <0.01, ***P <0.001 in two-tail paired Student's t-test respect untreated (grey).

A

During EMT (T7 / UNT)	Exon inclusion	H3K27me3 levels (ChIP)	H3K27ac levels (ChIP)	H3K4me1 levels (ChIP)	H3K36me3 levels (ChIP)	Nucleosome occupancy (MNAse)	RNA Pol II kinetics (DRB+RT-qPCR)	RNA Pol II levels (ChIP)	PTB dependent (shRNA)
CTNND1.exon 2	↑	↑	↓	↓	-	-	↓	↑	Yes
FGFR2.IIIc	↑	↓	↑	↑	↑T1 ↓T7 (1)	-	↓	↑	Yes
TCF7L2.exon 4	↓	↓	↑	↑	-	-	-	↓	Yes
SLK.exon 13	↓	↓	↓	↑	-	-	-	↓	Yes
SCRIB.exon 16	↑	↑	-	-	-	-	↓	↑	Yes
ENAH.exon 11	↓	-	-	-	-	-	-	-	Yes

B

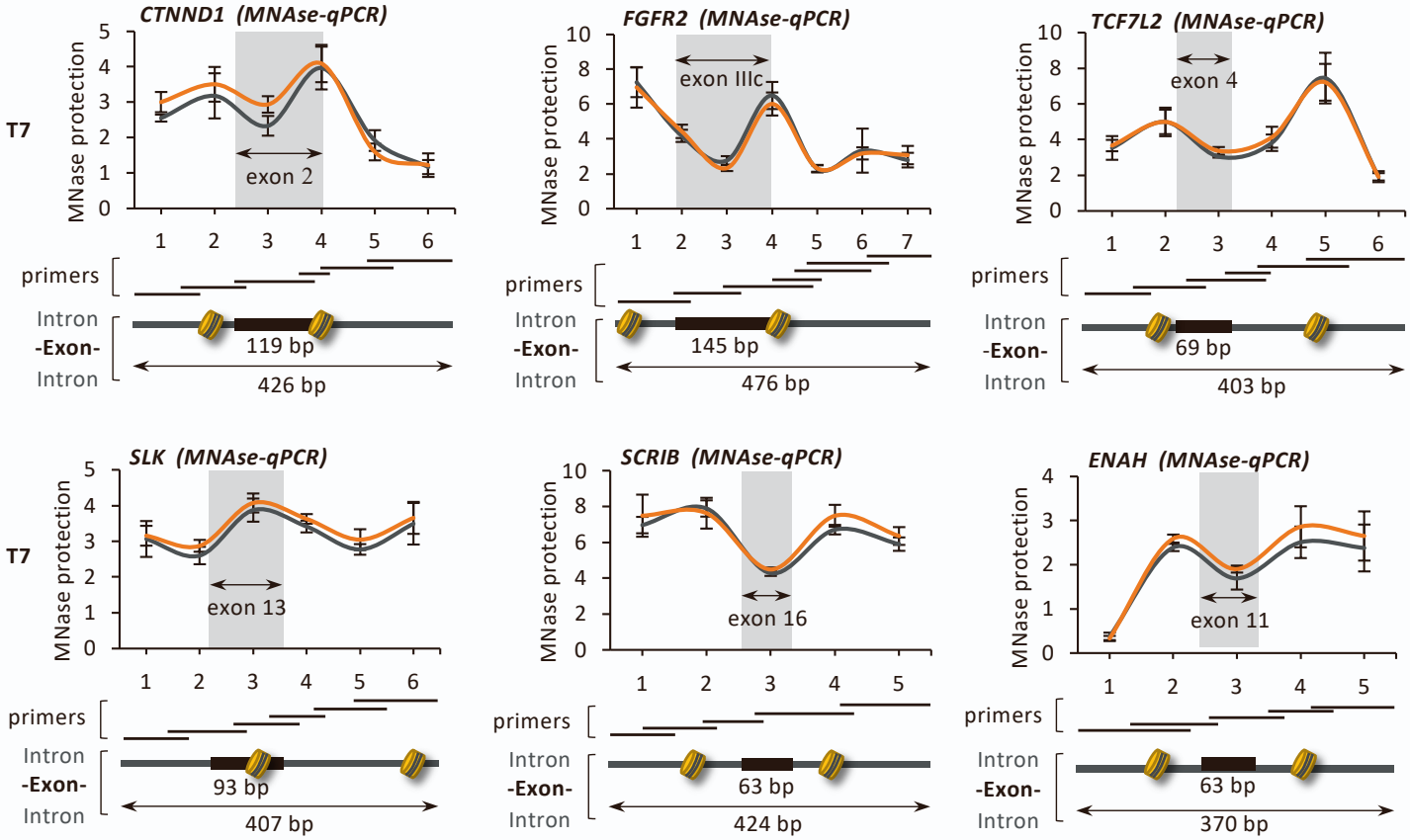

C

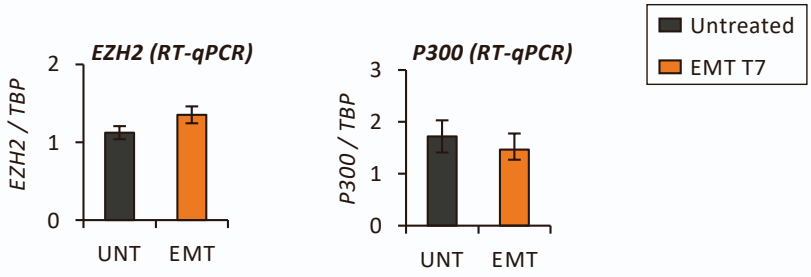

Figure S2. Summary of chromatin features defining alternatively spliced exons during EMT, related to Figure 1, 2 and S1. (**A**) Summary of the changes during EMT in exon inclusion, H3K27me3, H3K27ac, H3K4me1, H3K36me3, RNA Pol II enrichment levels, nucleosome occupancy, RNA Pol II kinetics and changes in splicing upon PTB knock-down at the studied exons. Arrows point to an increase or decrease in EMT-induced cells (T7) compared to untreated (UNT). A line indicates no significant change. [(1)] In T1, we observe changes in H3K36me3 levels just at the alternatively spliced exon IIIc. However in T7, there is a decrease in H3K36me3 levels all along the gene that corresponds to a dramatic repression of the gene at precisely this time-point, and it is thus independent of changes in splicing (75% reduction in overall gene expression levels). (**B**) MNAse protection assay to quantify changes in nucleosome positioning at *CTNND1*, *FGFR2*, *TCF7L2*, *SLK*, *SCRIB* and *ENAH* alternatively spliced exons in untreated and tamoxifen-induced MCF10a-Snail-ER cells for 7 days (T7) by qPCR (mean +/- SEM, n=4). Nucleosome positioning and location of the primers used are shown in graphical schemes. (**C**) Expression levels of *EZH2* and *P300,* relative to *TBP,* in untreated and EMT-induced (T7) cells by RT-qPCR (mean +/- SEM, n=9).

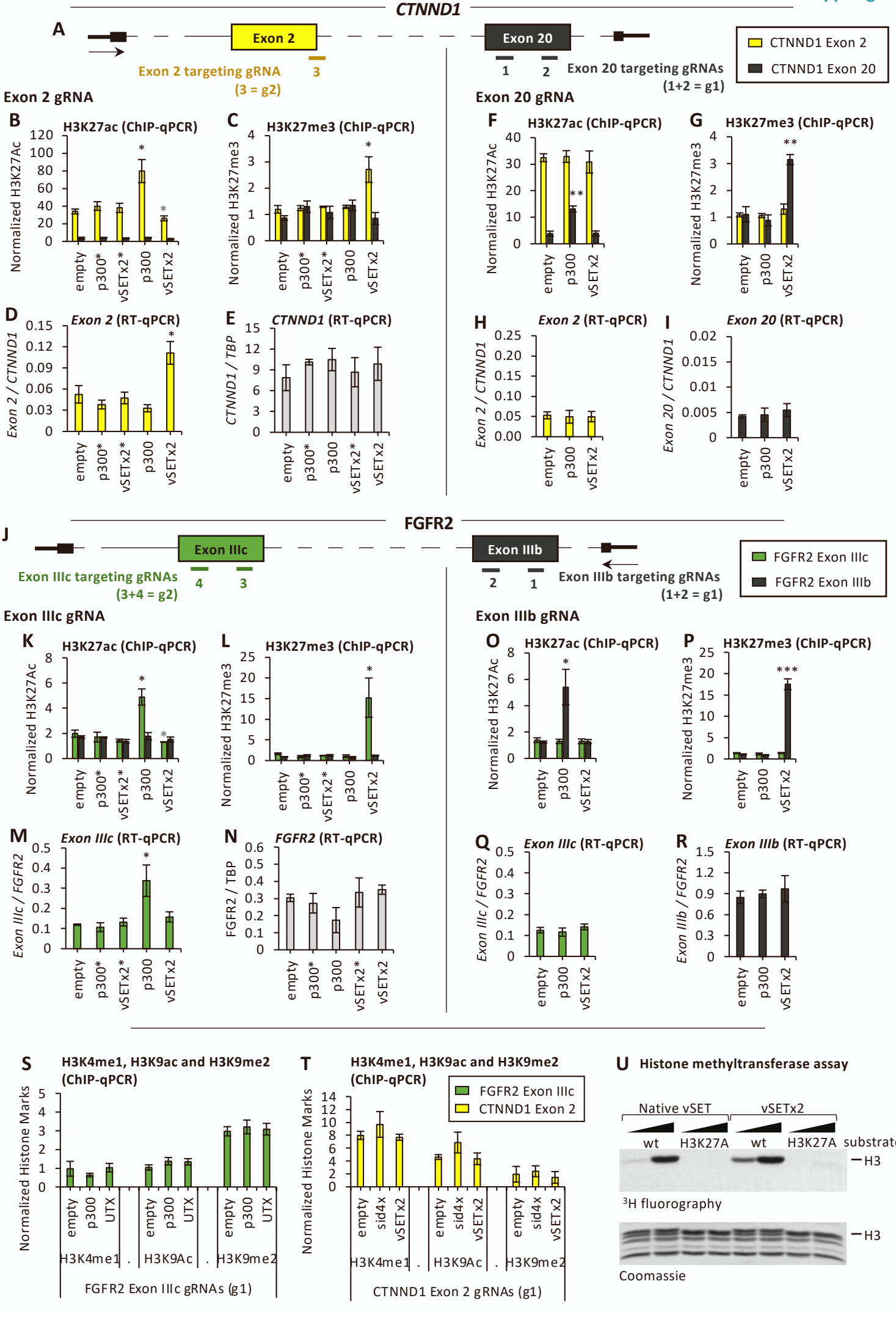
CTNND1
A
Exon 2
Exon 20
Exon 2 targeting gRNA (3 = g2)
Exon 20 targeting gRNAs (1+2 = g1)
CTNND1 Exon 2
CTNND1 Exon 20
Exon 2 gRNA
Exon 20 gRNA
B H3K27ac (ChIP-qPCR)
C H3K27me3 (ChIP-qPCR)
F H3K27ac (ChIP-qPCR)
G H3K27me3 (ChIP-qPCR)
Normalized H3K27Ac
Normalized H3K27me3
D Exon 2 (RT-qPCR)
E CTNND1 (RT-qPCR)
H Exon 2 (RT-qPCR)
I Exon 20 (RT-qPCR)
Exon 2 / CTNND1
CTNND1 / TBP
Exon 20 / CTNND1
empty
p300*
vSETx2*
p300
vSETx2
FGFR2
J
Exon IIIc
Exon IIIb
Exon IIIc targeting gRNAs (3+4 = g2)
Exon IIIb targeting gRNAs (1+2 = g1)
FGFR2 Exon IIIc
FGFR2 Exon IIIb
Exon IIIc gRNA
Exon IIIb gRNA
K H3K27ac (ChIP-qPCR)
L H3K27me3 (ChIP-qPCR)
O H3K27ac (ChIP-qPCR)
P H3K27me3 (ChIP-qPCR)
M Exon IIIc (RT-qPCR)
N FGFR2 (RT-qPCR)
Q Exon IIIc (RT-qPCR)
R Exon IIIb (RT-qPCR)
Exon IIIc / FGFR2
FGFR2 / TBP
Exon IIIb / FGFR2
S H3K4me1, H3K9ac and H3K9me2 (ChIP-qPCR)
T H3K4me1, H3K9ac and H3K9me2 (ChIP-qPCR)
Normalized Histone Marks
empty
p300
UTX
sid4x
vSETx2
H3K4me1
H3K9Ac
H3K9me2
FGFR2 Exon IIIc gRNAs (g1)
CTNND1 Exon 2 gRNAs (g1)
U Histone methyltransferase assay
Native vSET
vSETx2
wt
H3K27A
substrate
H3
3H fluorography
Coomassie

Figure S3. Exon-specific epigenome editing of H3K27 marks is sufficient to induce a change in splicing, related to Figure 3. (**A**) Schematic representation of *CTNND1* gene locus and the alternatively spliced exon 2 (yellow) and control exon 20 (grey) with the position of the gRNAs used to exon-specifically target the different dCas9 modifiers. (**B,C,F,G**) Enrichment levels of H3K27ac (B,F) and H3K27me3 (C,G) at *CTNND1* exon 2 (yellow) and control exon 20 (grey) in MCF10a-Snail-ER cells infected with dCas9 modifiers and exon-specific gRNAs targeting exon 2 (g2, which is a different combination from the one used in Figure 2) or exon 20 (g1) (mean +/- SEM, n=3). The percentage of input was normalized by two control regions across the different conditions. (**D,E,H,I**) Expression levels of *CTNND1* exon 2 (D,H), total *CTNND1* (E) and exon 20 (I) in untreated MCF10a-Snail-ER cells infected with dCas9 modifiers and the exon-specific gRNAs targeting exon 2 (g2) or exon 20 (g1). RT-qPCR values were normalized by total *CTNND1* or *TBP* as indicated in the graph (mean +/- SEM, n=4). (**J**) Schematic representation of *FGFR2* locus, with gRNAs position at the alternatively spliced exon IIIc (green) and control IIIb (grey). (**K,L,O,P**) Enrichment levels of H3K27ac (K,O) and H3K27me3 (L,P) at exon IIIc (green) and control exon IIIb (grey) in MCF10a-Snail-ER cells infected with dCas9 modifiers exon-specific gRNAs targeting IIIc (g2, which is a different combination from the one used in Figure 2) or IIIb (g1) (mean +/- SEM, n=4). The percentage of input was normalized by two control regions across the different conditions. (**S,T**) Enrichment levels of H3K4me1, H3K9ac and H3K9me2 at *FGFR2* exon IIIc (S, green) or *CTNND1* exon 2 (T, yellow) in untreated MCF10a-Snail-ER cells infected with dCas9 modifiers and exon-specific gRNAs targeting exon IIIc (g1) or exon 2 (g1) by ChIP-qPCR (mean +/- SEM, n=3). The percentage of input was normalized by two control regions across the different conditions. (**U**) Representative histone methyltransferase assay to show the specificity of native vSET and vSET2x activity on H3K27 residue in wild-type and H3K27A mutated recombinant chromatin templates. *P <0.05, **P <0.01, ***P <0.001 in two-tail paired Student's t-test respect empty dCas9 plasmid (empty). Black asterisks show a significant increase, while grey asterisks show a significant decrease in H3K27me3 or H3K27ac levels.

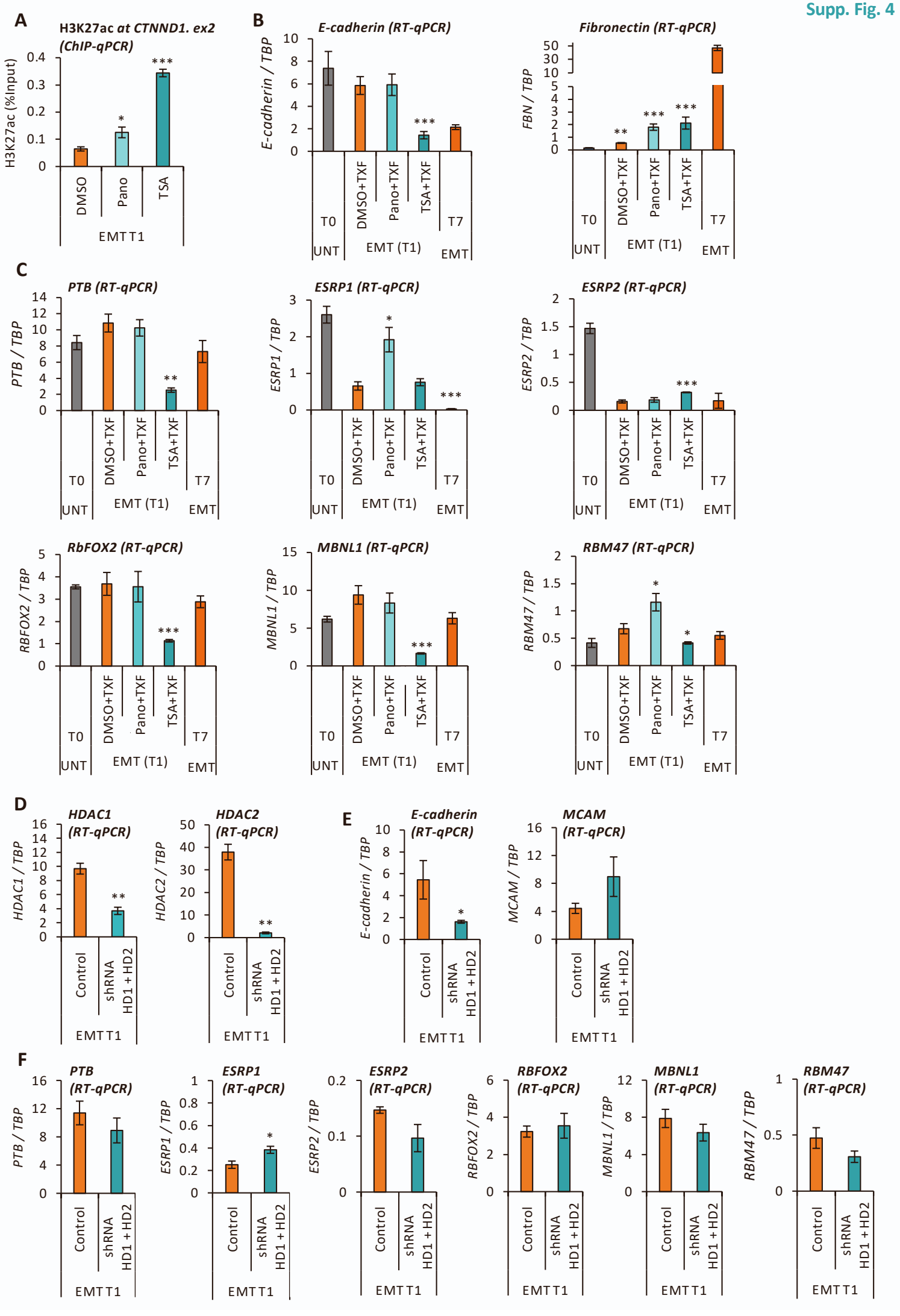
A
H3K27ac at CTNND1. ex2 (ChIP-qPCR)
H3K27ac (%Input)
DMSO
Pano
TSA
EMT T1
B
E-cadherin (RT-qPCR)
E-cadherin / TBP
Fibronectin (RT-qPCR)
FBN / TBP
T0
DMSO+TXF
Pano+TXF
TSA+TXF
T7
UNT
EMT (T1)
EMT
C
PTB (RT-qPCR)
PTB / TBP
ESRP1 (RT-qPCR)
ESRP1 / TBP
ESRP2 (RT-qPCR)
ESRP2 / TBP
RbFOX2 (RT-qPCR)
RBFOX2 / TBP
MBNL1 (RT-qPCR)
MBNL1 / TBP
RBM47 (RT-qPCR)
RBM47 / TBP
D
HDAC1 (RT-qPCR)
HDAC1 / TBP
HDAC2 (RT-qPCR)
HDAC2 / TBP
Control
shRNA HD1 + HD2
EMT T1
E
E-cadherin (RT-qPCR)
E-cadherin / TBP
MCAM (RT-qPCR)
MCAM / TBP
F
PTB (RT-qPCR)
ESRP1 (RT-qPCR)
ESRP2 (RT-qPCR)
RBFOX2 (RT-qPCR)
MBNL1 (RT-qPCR)
RBM47 (RT-qPCR)

Figure S4. Impact of HDAC inhibition in H3K27 marks and major splicing regulators, related to Figure 3. (**A**) Enrichment levels of H3K27ac at *CTNND1* exon 2 in MCF10a-Snail-ER cells treated for 24h with vehicle DMSO, 10nM of Pano (Panobinostat) or 3µg/mL of TSA (Trichostatin A) during EMT induction with tamoxifen. ChIP-qPCR data is shown as the percentage of input (mean +/- SEM, n=3). (**B-C**) Expression levels of epithelial (*E-cadherin*) and mesenchymal (*Fibronectin*) markers and key EMT splicing factors in MCF10a-Snail-ER cells treated for 24h with vehicle DMSO, 10nM of Pano (Panobinostat) or 3µg/mL of TSA (Trichostatin A) during EMT induction with tamoxifen. Untreated (T0) and fully induced EMT cell (T7) are shown as control references. RT-qPCR data was normalized by *TBP* (mean +/- SEM, n=3). **(D, E, F)** Expression levels of *HDAC1*, *HDAC2*, EMT markers and splicing factors upon double knock-down of *HDAC1* (*HD1*) and *HDAC2* (*HD2*) in MCF10a-Snail-ER cells induced for EMT during 24h. Non-mammalian targeting shRNA was used as a control. RT-qPCR data was normalized by *TBP* (mean +/- SEM, n=3). *P <0.05, **P <0.01, ***P <0.001 in two-tail paired Student's t-test respect T1 DMSO or T1 non-targeting shRNA (control).

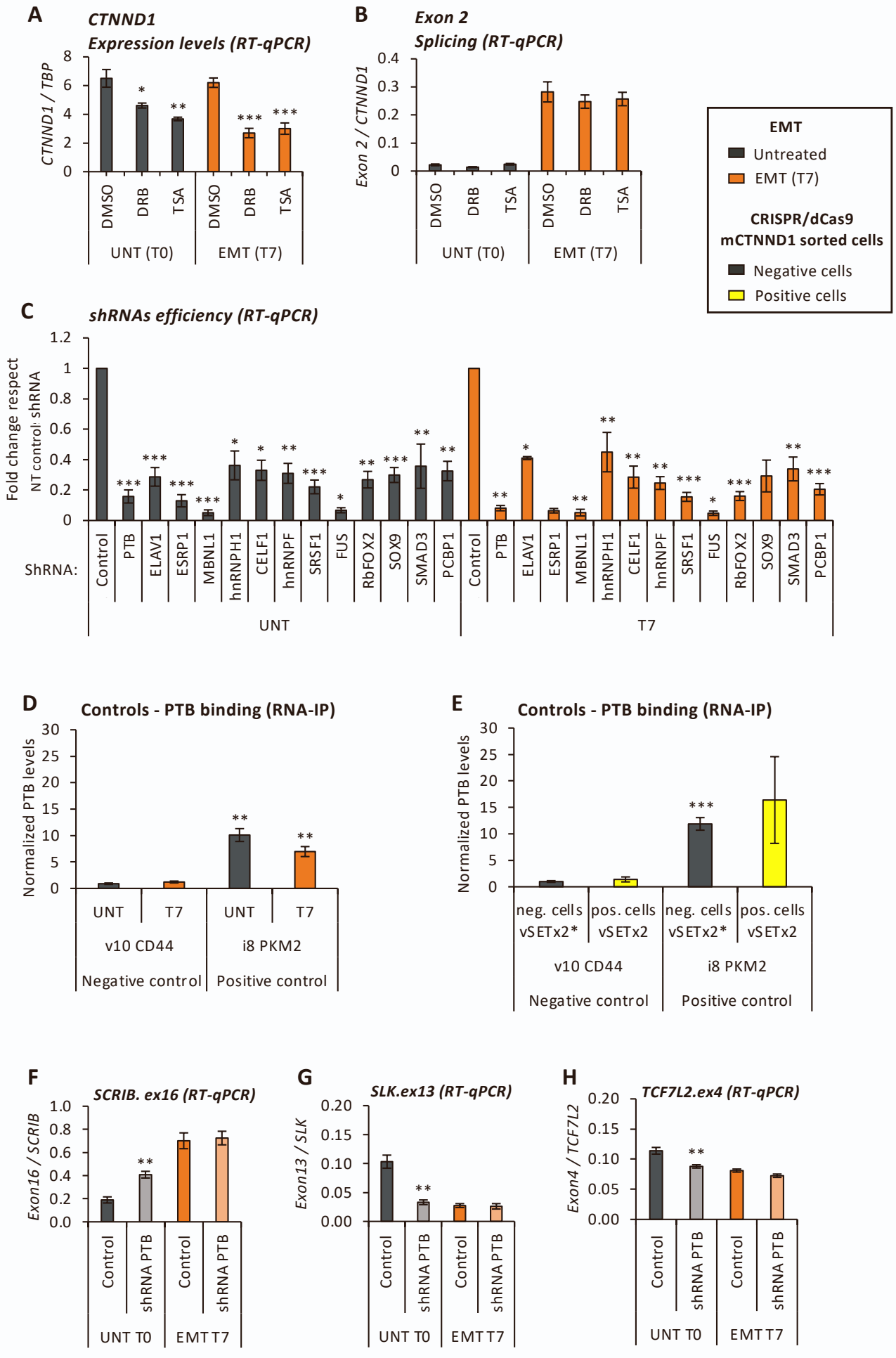
A
CTNND1
Expression levels (RT-qPCR)
CTNND1 / TBP
DMSO
DRB
TSA
UNT (T0)
EMT (T7)
B
Exon 2
Splicing (RT-qPCR)
Exon 2 / CTNND1
EMT
Untreated
EMT (T7)
CRISPR/dCas9
mCTNND1 sorted cells
Negative cells
Positive cells
C
shRNAs efficiency (RT-qPCR)
Fold change respect
NT control shRNA
ShRNA:
Control
PTB
ELAV1
ESRP1
MBNL1
hnRNPH1
CELF1
hnRNPF
SRSF1
FUS
RbFOX2
SOX9
SMAD3
PCBP1
UNT
T7
D
Controls - PTB binding (RNA-IP)
Normalized PTB levels
UNT
T7
v10 CD44
i8 PKM2
Negative control
Positive control
E
Controls - PTB binding (RNA-IP)
Normalized PTB levels
neg. cells vSETx2*
pos. cells vSETx2
v10 CD44
i8 PKM2
Negative control
Positive control
F
SCRIB. ex16 (RT-qPCR)
Exon16 / SCRIB
Control
shRNA PTB
UNT T0
EMT T7
G
SLK.ex13 (RT-qPCR)
Exon13 / SLK
H
TCF7L2.ex4 (RT-qPCR)
Exon4 / TCF7L2

Figure S5. H3K27 marks regulate splicing by modulating the recruitment of the splicing factor PTB, related to Figure 4. (**A,B**) *CTNND1* and exon 2 expression levels normalized by total *TBP* or *CTNND1* levels, respectively, in tamoxifen-untreated epithelial (UNT, grey) and EMT-induced (T7, orange) MCF10a-Snail-ER cells co-treated with DMSO (control), 1 μg/mL TSA (HDAC inhibitor) or 40μM DRB (RNA Polymerase II inhibitor) for 24h. RT-qPCR results are shown as the mean +/- SEM of n=4 biological replicates. (**C**) Total expression levels of the candidate splicing factors involved in *CTNND1* exon 2 regulation upon shRNA knockdown in untreated (UNT, grey) and tamoxifen-induced (T7, orange) MCF10a-Snail-ER cells. RT-qPCR levels are shown relative to cells infected with non-mammalian targeting control shRNA (mean +/- SEM, n=3). (**D**) PTB enrichment levels at the the negative control *CD44 v10* and positive control *PKM2 intron 8* in untreated (UNT) and tamoxifen-induced (T7) MCF10a-Snail-ER cells. The percentage of input of UV-crosslinked RNA immunoprecipitations were normalized by IgG and *CTNND1 exon 7* control levels as in Figure 3 (mean ± SEM, n=5). (**E**) PTB enrichment levels at the same positive and negative control regions as in (D) in cell-sorted MCF10-Snail-ER cells expressing (positive) or not (negative) the mesenchymal-specific splicing isoform mCTNND1(ex2) upon infection with dCas9-vSETx2, or mutant dCas9-vSETx2*, and the exon-specific gRNAs (g1) targeting *CTNND1 exon 2*. The percentage of input of UV-crosslinked RNA immunoprecipitations were normalized by IgG and *CTNND1 exon 7* control levels (mean ± SEM, n=4). (**F-H**) Inclusion levels of the indicated exons relative to the total expression levels of their corresponding gene upon shRNA knock-down of PTB in epithelial untreated (UNT T0, grey) and tamoxifen-induced (EMT T7, orange) MCF10a-Snail-ER cells. Non-mammalian targeting shRNA is used as a control (mean +/- SEM, n=4). *P <0.05, **P <0.01, ***P <0.001 in two-tail paired Student's t-test respect the negative control *CD44 v10 or* cells infected with non-targeting shRNA.

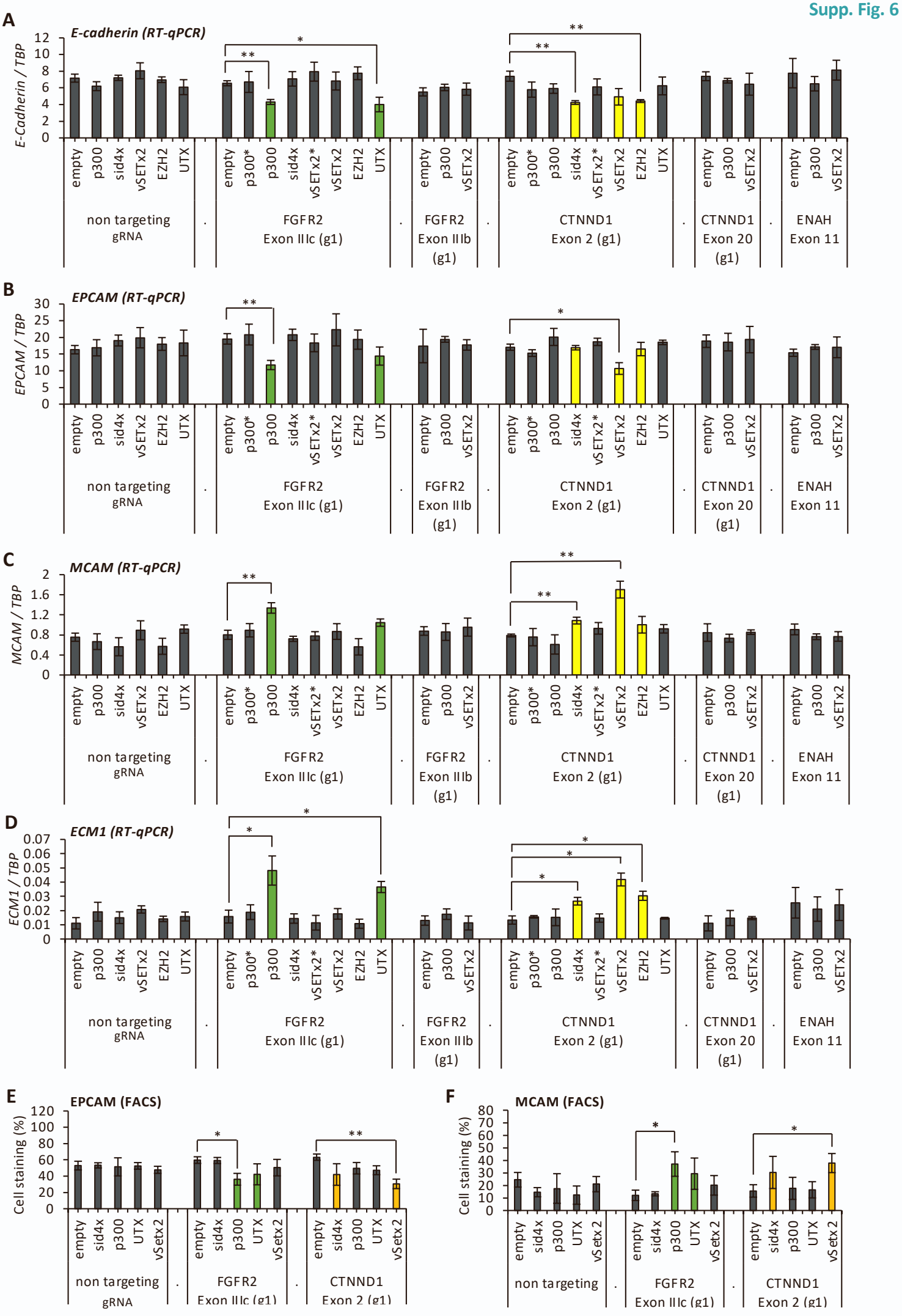
A
E-cadherin (RT-qPCR)
E-Cadherin / TBP
B
EPCAM (RT-qPCR)
EPCAM / TBP
C
MCAM (RT-qPCR)
MCAM / TBP
D
ECM1 (RT-qPCR)
ECM1 / TBP
empty
p300
sid4x
vSETx2
EZH2
UTX
p300*
vSETx2*
non targeting gRNA
FGFR2 Exon IIIc (g1)
FGFR2 Exon IIIb (g1)
CTNND1 Exon 2 (g1)
CTNND1 Exon 20 (g1)
ENAH Exon 11
E
EPCAM (FACS)
Cell staining (%)
vSetx2
F
MCAM (FACS)

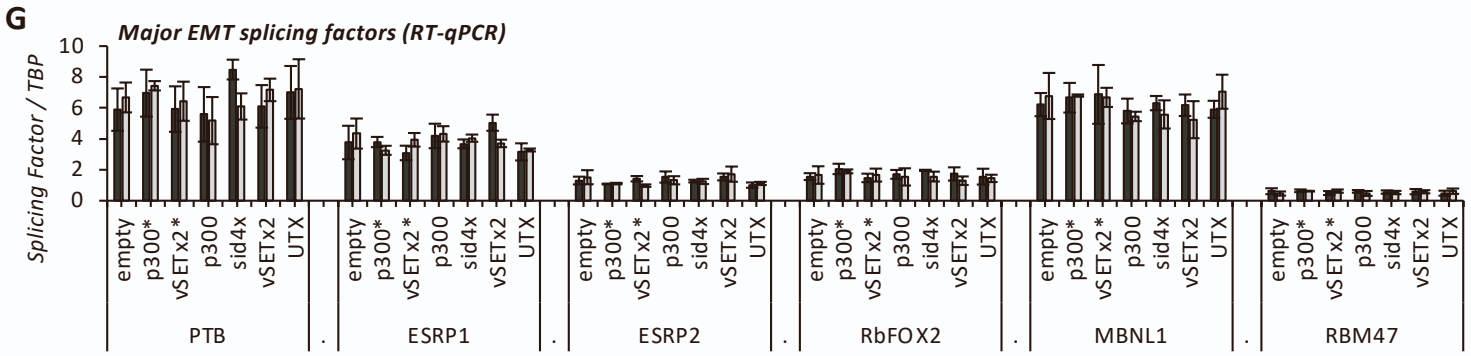
G
Major EMT splicing factors (RT-qPCR)
Splicing Factor / TBP
empty
p300*
vSETx2*
p300
sid4x
vSETx2
UTX
PTB
ESRP1
ESRP2
RbFOX2
MBNL1
RBM47

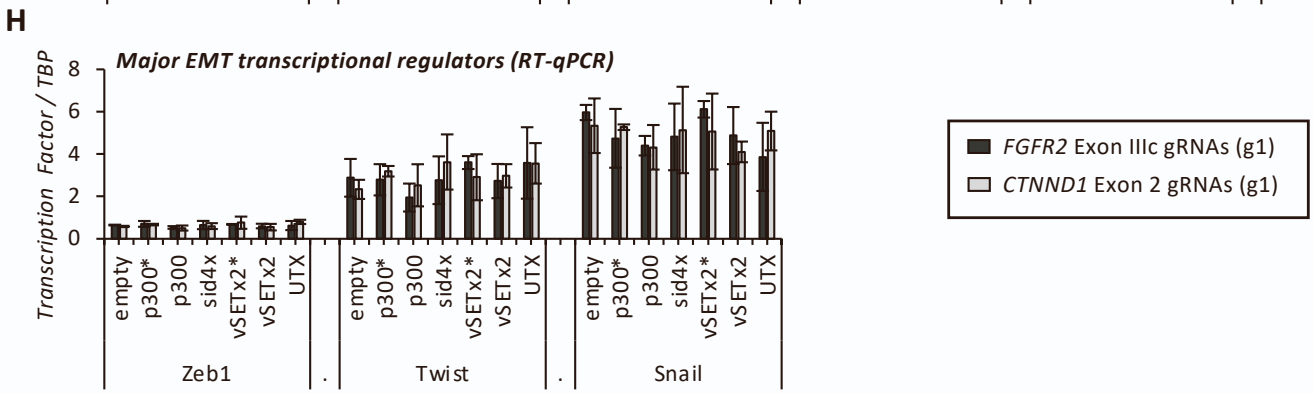
H
Major EMT transcriptional regulators (RT-qPCR)
Transcription Factor / TBP
Zeb1
Twist
Snail
FGFR2 Exon IIIc gRNAs (g1)
CTNND1 Exon 2 gRNAs (g1)

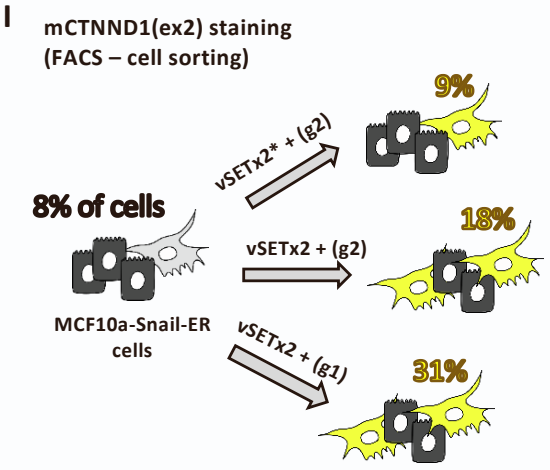
I
mCTNND1(ex2) staining
(FACS – cell sorting)
8% of cells
MCF10a-Snail-ER cells
vSETx2* + (g2)
vSETx2 + (g2)
vSETx2 + (g1)
9%
18%
31%

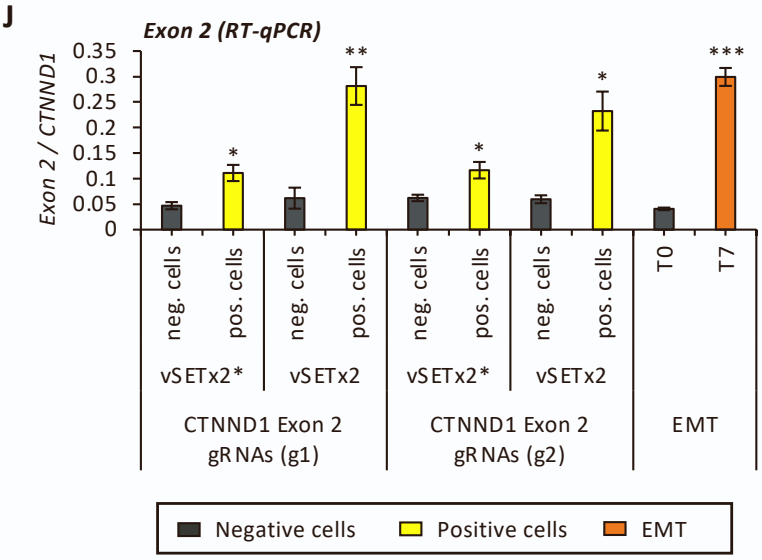
J
Exon 2 (RT-qPCR)
Exon 2 / CTNND1
neg. cells
pos. cells
vSETx2*
vSETx2
T0
T7
CTNND1 Exon 2 gRNAs (g1)
CTNND1 Exon 2 gRNAs (g2)
EMT
Negative cells
Positive cells
EMT

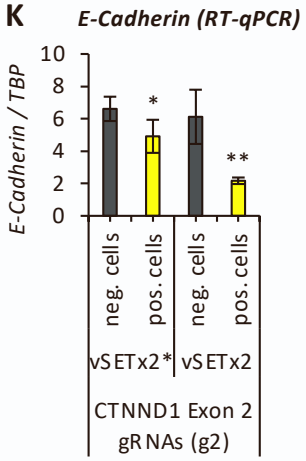
K
E-Cadherin (RT-qPCR)
E-Cadherin / TBP
CTNND1 Exon 2 gRNAs (g2)

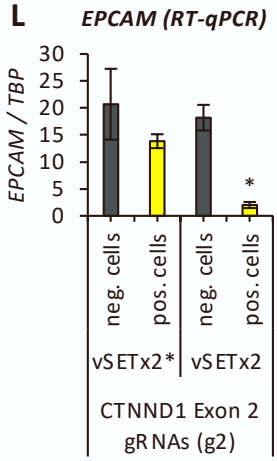
L
EPCAM (RT-qPCR)
EPCAM / TBP
CTNND1 Exon 2 gRNAs (g2)

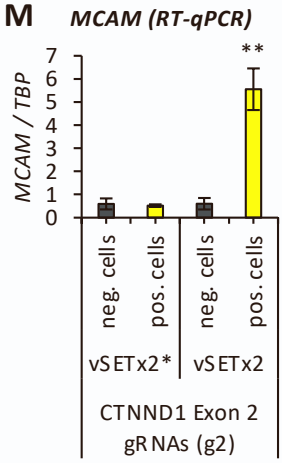
M
MCAM (RT-qPCR)
MCAM / TBP
CTNND1 Exon 2 gRNAs (g2)

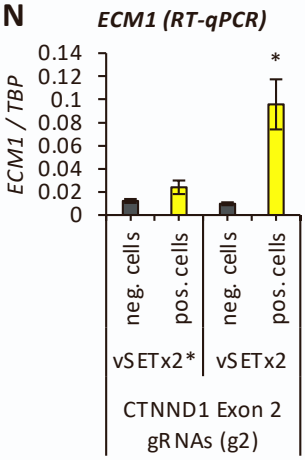
N
ECM1 (RT-qPCR)
ECM1 / TBP
CTNND1 Exon 2 gRNAs (g2)

Figure S6. Direct effect of dCas9 epigenomic editing on EMT, related to Figure 5. (**A-F**) Changes in expression levels, at the mRNA (A-D) and protein level (E-F), of epithelial (*E-Cadherin*, *EPCAM*) and mesenchymal (*MCAM*, *ECM1*) markers in MCF10a-Snail-ER cells infected with different dCas9 modifiers and exon-specific gRNAs targeting *FGFR2* exon IIIc (g1), *FGFR2* exon IIIb (g1), *CTNND1* exon 2 (g1), *CTNND1* exon 20 (g1) or *ENAH* exon 11. A non-targeting gRNA was used as a negative control. RT-qPCR levels were normalized by *TBP,* whereas protein levels were quantified by FACS using as background levels results obtained with no primary antibody (mean +/- SEM, n=3). In green, there are highlighted the conditions in which there is a change in *FGFR2*.IIIc splicing and in yellow when there is a change in *CTNND1*.ex2 splicing. (**G,H**) Expression levels of the splicing factors (*PTB*, *ESRP1*, *ESRP2*, *RBFOX2*, *MBNL1* and *RBM47*) and transcriptional regulators (*Zeb1*, *Twist1* and *Snail1*) most important for EMT in MCF10a-Snail-ER cells infected with different dCas9 modifiers and exon-specific gRNAs targeting *FGFR2* exon IIIc (g1, dark grey) or *CTNND1* exon 2 (g1, light grey). RT-qPCR levels were normalized by *TBP* (mean +/- SEM, n=3). (**I**) MCF10a-Snail-ER cells infected with dCas9-vSETx2 or mutant dCas9-vSETx2* and two different combinations of exon-specific gRNAs (g1 and g2) targeting *CTNND1* exon 2 were cell-sorted by expression levels of the mesenchymal CTNND1 protein variant, which includes exon 2 (mCTNND1(ex2)), using splicing-specific antibodies. Negative cells not expressing mCTNND1(ex2) and tamoxifen-induced T7 EMT cells were used as controls. The percentage of mCTNND1(ex2) positive cells per condition is shown. (**J**) *CTNND1* exon 2 inclusion levels in cells expressing (positive) or not (negative) the splicing variant mCTNND1(ex2) in the conditions described in (I). RT-qPCR levels were normalized by total *CTNND1* expression levels (mean +/- SEM, n=3). (**K-N**) Expression levels of epithelial (*E-Cadherin*, *EPCAM*) and mesenchymal (*MCAM*, *ECM1*) markers in cell-sorted MCF10a-Snail-ER cells infected with dCas9-vSETx2 or the mutant dCas9-vSETx2* and the second combination (g2) of gRNAs targeting *CTNND1 exon2*. RT-qPCR levels were normalized by *TBP* expression levels (mean +/- SEM, n=3). *P <0.05, **P <0.01, ***P <0.001 in two-tail paired Student's t-test respect respect the corresponding control: empty dCas9 or cell sorted cells negative for expression of mCTNND1(ex2).